

Explicit Credit Assignment through Local Rewards and Dependence Graphs in Multi-Agent Reinforcement Learning

Bang Giang Le¹ Viet Cuong Ta¹

Abstract

To promote cooperation in Multi-Agent Reinforcement Learning, the reward signals of all agents can be aggregated together, forming global rewards that are commonly known as the fully cooperative setting. However, global rewards are usually noisy because they contain the contributions of all agents, which have to be resolved in the credit assignment process. On the other hand, using local reward benefits from faster learning due to the separation of agents' contributions, but can be suboptimal as agents myopically optimize their own reward while disregarding the global optimality. In this work, we propose a method that combines the merits of both approaches. By using a graph of interaction between agents, our method discerns the individual agent contribution in a more fine-grained manner than a global reward, while alleviating the cooperation problem with agents' local reward. We also introduce a practical approach for approximating such a graph. Our experiments demonstrate the flexibility of the approach, enabling improvements over the traditional local and global reward settings.

1. Introduction

Cooperation between multiple agents in Multi-Agent Reinforcement Learning (MARL) can be understood as the collective effort whereby multiple agents jointly pursue a shared objective, thereby achieving a better outcome that might be unattainable by individual agents alone. Such collaboration is crucial in real-world applications, where tasks such as autonomous driving (Shalev-Shwartz et al., 2016), distributed voltage control (Wang et al., 2021), or swarm coordination (Cao et al., 2012) are often too complex for isolated agents to solve effectively. As a result, Cooperative MARL remains a central research direction within multi-agent learning (Yuan et al., 2023).

¹VNU University of Engineering and Technology, Hanoi. Correspondence to: Viet Cuong Ta <cuongtv@vnu.edu.vn>.

The simplest approach to enforce cooperation within a group of agents is through reward aggregation (scalarization), where the rewards of individuals are replaced by the sum (average) of the agents' rewards in the whole group (Samvelyan et al., 2019; Lowe et al., 2017). In this way, all agents share a common objective, which is the reward of the whole group; the loss of the group is the loss of every agent. This setting generally goes under the name *fully cooperative* settings in the literature (Yu et al., 2022; Rashid et al., 2020b). Rewards scalarization, however, introduces the problem of *credit assignment* (Chang et al., 2003; Foerster et al., 2018), where the information on the contributions of each agent is lost through the scalarization operations.

Alternatively, in a general *cooperative* setting, individual rewards are kept separate, and each agent optimizes its own objective independently, which effectively reduces the Multi-agent problem to a set of single-agent RL tasks (De Witt et al., 2020). This learning approach is often referred to as *independent learning*, with examples including IQL (Tan, 1993), IPPO (De Witt et al., 2020), and MADDPG (Lowe et al., 2017). In this approach, each agent optimizes its own reward signal myopically, and therefore, agents only cooperate when cooperation is beneficial to them. In this case, cooperation can only emerge implicitly (Zheng et al., 2018). Learning from local rewards can potentially lead to selfish behaviors that can be suboptimal to the entire system (Devlin et al., 2014; Le & Ta, 2025).

In fully cooperative MARL, it is often assumed that all agents share a single global reward. To mitigate the resulting credit assignment problem, various methods have been proposed, such as value decomposition (Sunehag et al., 2017) and counterfactual learning (Foerster et al., 2018). However, in many scenarios, the team's reward can be naturally attributed to the contributions of specific subsets of agents, in which case local rewards can provide more fine-grained information about overall performance. Consequently, aggregating these signals into a single scalar and then attempting to recover them appears inherently inefficient. Motivated by this observation, we ask

Can we directly leverage the individual-agent reward information to effectively avoid the credit

assignment issues introduced by reward scalarization, while still promoting cooperation?

Building on the framework of dependence graphs and Multi-Agent Networked MDPs (Qu et al., 2020), we combine local reward signals in a way that respects the credit of each agent. Our main contributions in this work are two-fold. First, we propose a novel policy gradient estimator that truncates irrelevant local rewards based on interaction paths in the dependence graph, effectively alleviating the credit assignment problem. Second, we introduce a practical method for approximating the dependence graph, along with a GAE-based advantage estimator (Schulman et al., 2015) that can work effectively with noisy graph approximations. Empirically, we validate the proposed approach on a range of benchmarks in MARL. Experimental results show that our methods can be competitive with and outperform strong baselines from both local and global reward settings.

2. Related Work

Reward for Cooperation. The behaviors of RL agents are defined by the reward structure, a principle known as the reward hypothesis (Sutton & Barto, 2018). Effective reward functions are notoriously difficult to design, and this remains true in cooperative MARL (Pan et al., 2022). Traditionally, agents are trained using separate, agent-specific reward vectors under the independent learning framework, where each agent is treated as an individual RL problem (Tan, 1993; De Witt et al., 2020). This approach offers benefits such as simplicity and scalability (Oroojlooy & Hajinezhad, 2023), but also suffers from issues like non-stationarity and miscoordination (Hernandez-Leal et al., 2017). The degree of cooperation is also sensitive to reward shapings (Leibo et al., 2017; Tampuu et al., 2017).

In contrast, using a shared reward function directly enforces cooperation as in fully cooperative MARL settings (Yuan et al., 2023). This setup is often trained under the Centralized Training with Decentralized Execution (CTDE) paradigm (Foerster et al., 2018), which further enhances coordination through centralized training. However, shared rewards introduce the credit assignment problem, making it difficult to scale fully cooperative learning to environments with many agents (Bagnell & Ng, 2005; Wang et al., 2020d). As a result, local reward learning is more suitable for large-scale MARL problems (Zheng et al., 2018).

Recently, a number of approaches attempt to explore a middle ground between the two aforementioned reward settings. For instance, Le & Ta (2025) apply tools from multi-objective optimization to identify Pareto optimal policies. However, their method treats the problem as a generic optimization task and does not explicitly model individual agent contributions within the sequential decision-making process.

Wang et al. (2022) optimize auxiliary local rewards alongside the sparse global team reward. However, ultimately this approach still solves the two different reward formulations and relies on additional heuristic design of local rewards to enable effective learning.

Credit assignment. Credit assignment problem is the problem of attributing the contribution of individual agents from the team’s rewards (Chang et al., 2003). Two main approaches to solving credit assignment problems in the literature include (i) decomposing the global value function, and (ii) marginalizing the contribution of one agent over the others (Gronauer & Diepold, 2022). The first approach, sometimes referred to as implicit credit assignment (Zhou et al., 2020), has gained popularity from the works of VDN (Sunehag et al., 2017) and QMIX (Rashid et al., 2020b). This approach is characterized by using individual utility functions and a mixing procedure to combine them into a total joint value function. To facilitate efficient decentralized execution, most methods follow the Individual-Global-Max (IGM) principle (Hong et al., 2022). IGM ensures local greedy agents align with globally optimal actions, but in practice, its limited decomposability can hinder convergence (Wang et al., 2020a; Rashid et al., 2020a). Coordination Graph (Guestrin et al., 2001) provides another approach that factorizes the joint value function using a graph structure, enabling a higher-order value factorizations (Kok & Vlassis, 2006). However, this method introduces significant computational overhead, which in practice often restricts implementations to pairwise interactions (Böhmer et al., 2020). The second approach, with representative works such as Counterfactual learning (Foerster et al., 2018), mainly uses baselines (Weaver & Tao, 2013; Wu et al., 2018) to reduce the variance of Policy Gradient estimation (Kuba et al., 2021). Shapley Q-value (Wang et al., 2020c) is a similar approach that assigns credit based on agents’ average marginal contribution over all coalition formations. A common characteristic of these methods is that they start from the global reward and distribute credit in a top-down manner. In contrast, our work avoids the credit assignment problem by directly using local rewards in a bottom-up approach.

Networked Multi-Agent MDPs. Theoretically, our formulation is related to the works that model agent interactions as a networked graph in the Multi-Agent MDP framework (Qu & Li, 2019; Qu et al., 2020). This formulation enables more fine-grained modeling of local interactions, which is useful for analyzing agents’ contributions. Most works in this direction rely on the exponential decay property of value representations (Lin et al., 2021) to approximate the value function using a small subset of agents, possibly with communications (Ma et al., 2024). Our work explores the time dimension of value estimation along the dependency graph paths, which places our approach closer to the credit assignment problem in this framework.

3. Problem Setting and Notation

Markov Game. We formulate the MARL problem as a Markov game, defined by the tuple $\mathcal{M} = \langle \mathcal{N}, \mathcal{S}, \mathcal{A}, \mathbf{P}, \mathbf{r}, \gamma \rangle$. Here, $\mathcal{N} = \{1, 2, \dots, N\}$ denotes the set of N agents, \mathcal{S} is the state space, and $\mathcal{A} = \mathcal{A}_1 \times \dots \times \mathcal{A}_N$ represents the joint action space, where \mathcal{A}_i is the action space of agent i . The function \mathbf{P} defines the transition dynamics, $\mathbf{r} : \mathcal{S} \times \mathcal{A} \rightarrow [0, R_{\max}]^N$ is the joint reward function, and $\gamma \in [0, 1)$ is the discount factor. Throughout the paper, we use bold notation to indicate joint quantities: for example, the joint action at time step t is denoted by $\mathbf{a}_t = (a_t^1, \dots, a_t^N)$, and the joint policy by $\boldsymbol{\pi} = (\pi_1, \dots, \pi_N)$. At each time step t , all agents independently select actions according to their policies, forming the joint action \mathbf{a}_t , upon which the environment transitions to the next state s_{t+1} according to the transition kernel \mathbf{P} . Additionally, let $\rho_{\boldsymbol{\pi}}(\mathbf{s}) = \sum_{t=0}^{\infty} \gamma^t \mathbb{P}_{\boldsymbol{\pi}}(\mathbf{s}_t = \mathbf{s})$ be the improper marginal state distribution.

Networked Multi-Agent MDP. Many practical MARL problems exhibit local dependence structures, where agents may interact with a small subset of neighbors and are relatively independent of other outsider agents. To facilitate such structural dependency, we utilize the framework of networked Markov systems (Qu & Li, 2019; Qu et al., 2020). More specifically, we assume that the joint state space \mathcal{S} can be decomposed into substate spaces of individual agents, i.e., $\mathcal{S} = \mathcal{S}_1 \times \dots \times \mathcal{S}_N$, and an agent can only observe their respective substates, $\pi_i : \mathcal{S}_i \rightarrow \Delta(\mathcal{A}_i)$. The transition kernel \mathbf{P} also factorizes accordingly: the next state of agent i depends only on a local agent-dependence set, denoted by $\text{Pa}_{\mathbf{P}}^i(s^i) \subseteq \mathcal{N}$, with

$$P_i(s^{i'}|\mathbf{s}, \mathbf{a}) = P_i(s^{i'} \mid \{s^k, a^k : k \in \text{Pa}_{\mathbf{P}}^i(s^i)\}) \in \Delta(\mathcal{S}_i).$$

Note that the agent dependence set depends on the local states; agents can infer from their observations which other agents can affect their next state. We assume $i \in \text{Pa}_{\mathbf{P}}^i(s^i)$, that is, each agent always influences its own next state. This decomposition structure naturally forms a *(state-)dependence graph*, which we define later in this section.

Each agent i also receives an individual reward $r^i : \mathcal{S}_i \times \mathcal{A}_i \rightarrow [0, R_{\max}]$ based on their states and actions. For clarity of exposition in the main text, we restrict to the case where r^i depends only on the local state-action pair (s^i, a^i) . More general settings of the reward functions can be naturally captured by introducing a second *reward-dependence graph*. The reward-dependence graph captures myopic interactions: the immediate effect to current rewards, future propagation is already captured by the state-dependence graph. Since this extension does not alter the main theory and can be incorporated with minor modifications, we defer its full formalization to Appendix A.6.

We define the cumulative returns of agent i under the joint

policy $\boldsymbol{\pi}$ as $\mathcal{J}^i(\boldsymbol{\pi}) = \mathbb{E}_{\boldsymbol{\pi}} \left[\sum_{t=0}^{\infty} \gamma^t r_t^i \right]$. In the fully cooperative setting, agents optimize a shared objective by maximizing the team’s total expected return, $\mathcal{J}(\boldsymbol{\pi}) = \sum_{i=1}^N \mathcal{J}^i(\boldsymbol{\pi})$, with $r_t = \sum_{i=1}^N r_t^i$, where the scalarized reward r_t serves as a common learning signal for all agents. Throughout the paper, we refer to the scalarized reward r_t as *global reward* to distinguish it from the *local reward* r_t^i .

The factorization of the global states resembles the partial observability property, where each agent only observes parts of the underlying states. However, unlike partial observation, the transition kernel directly operates on the partial states. Furthermore, one can recover a vanilla formulation by duplicating the true states, $\mathbf{s} = (s, \dots, s)$, and by defining the transition kernel P_i to include all the agents in the set Pa_i^i . Our formulation differs from prior work in the underlying dependence structure. In Qu & Li (2019), the dependencies form a tree, which corresponds to a dependence set of size one in our framework. Qu et al. (2020) consider a graph-structured formulation, but the graph is fixed, whereas in our setting, the dependence graph is dynamic and can vary across states.

State Dependence Graph. Based on the Dependence structure, we define the dependence graph, in which a directed edge exists between two agents if one agent influences the other’s next states.

Definition 3.1 (State Dependence Graph induced by a Networked Multi-Agent MDP). Let \mathcal{M} be a Networked Multi-Agent MDP. The *State Dependence Graph* of \mathcal{M} is a directed graph $\mathcal{G} = \langle \mathcal{V}, \mathcal{E} \rangle$, where $\mathcal{V} = \{(\mathbf{s}, i) \mid \mathbf{s} \in \mathcal{S}, i \in [N]\}$ is the vertex set and \mathcal{E} is the edge set. A directed edge $(\mathbf{s}, i) \rightarrow (\mathbf{s}', j)$ belongs to \mathcal{E} if $i \in \text{Pa}_{\mathbf{P}}^j(s^j)$ and $\exists \mathbf{a} \in \mathcal{A}$ such that $\mathbf{P}(\mathbf{s}'|\mathbf{s}, \mathbf{a}) > 0$.

Definition 3.2 (Proper Dependence Graph). A graph $\mathcal{G} = \langle \mathcal{V}, \mathcal{E} \rangle$ is proper if there exists a transition kernel \mathbf{P} that admits it as a dependence graph; i.e. if $(\mathbf{s}_1, i) \rightarrow (\mathbf{s}'_1, j)$ and $(\mathbf{s}_2, i) \rightarrow (\mathbf{s}'_2, i)$ are two edges of \mathcal{G} such that $s_1^j = s_2^j$, then $(\mathbf{s}_2, i) \rightarrow (\mathbf{s}'_2, j)$ is also an edge of \mathcal{G} . Every proper dependence graph has a unique collection of agent-dependence sets $\{\text{Pa}_{\mathcal{G}}^i(s^i)\}_i^N$ for each state \mathbf{s} .

Definition 3.3 (Path in the Dependence Graph). Let $\mathcal{G} = \langle \mathcal{V}, \mathcal{E} \rangle$ be the induced Dependence Graph of \mathcal{M} . A *path* from vertex (\mathbf{s}, i) to vertex (\mathbf{s}', j) is a sequence of vertices

$$(\mathbf{s}_0, i_0) \rightarrow (\mathbf{s}_1, i_1) \rightarrow \dots \rightarrow (\mathbf{s}_L, i_L),$$

such that

1. $i_0 = i, i_L = j, \mathbf{s}_0 = \mathbf{s}, \mathbf{s}_L = \mathbf{s}'$,
2. for each $\ell = 0, \dots, L-1$, the directed edge $(\mathbf{s}_\ell, i_\ell) \rightarrow (\mathbf{s}_{\ell+1}, i_{\ell+1})$ belongs to \mathcal{E} .

We call L the *length* of the path. If there is a path from (\mathbf{s}_t, i) to $(\mathbf{s}_{t'}, j)$, then there is a path from (\mathbf{s}_t, i) to any of $(\mathbf{s}_{t''}, j)$

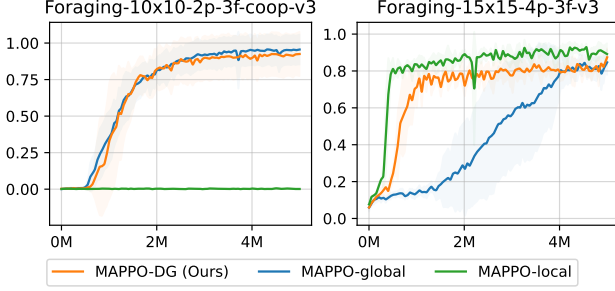


Figure 1. Reward dilemma in cooperative MARL; global reward enhances cooperation but introduces credit assignment problem, while local reward can induce suboptimal policies in the environments that require cooperation. Our method enables faster training, as in local rewards, while avoiding the miscoordination pitfall.

for all $t'' \geq t'$ since an agent influences its next states. A path is defined on a realizable sequence of state that we call a (state) trajectory.

Information-Theoretic Notation. We use capital letters to denote random variables corresponding to the same entities; for example, S^i and A^i represent the random variables associated with the (sub)state s^i and action a^i of the agent i . We also use $H(\cdot)$ to denote entropy and $I(\cdot; \cdot)$ to denote mutual information.

4. Motivation: Scalarize or not scalarize

Existing works in cooperative MARL either use a global reward, for example, in CTDE, or a local reward, such as in independent learning (see Section 2). However, these two setups represent two extreme learning paradigms that are only suitable on a case-by-case basis. To illustrate, we provide an example of these two learning modes in the LBF environments (Christianos et al., 2020). We demonstrate two scenarios that exhibit contrasting learning patterns on the same backbone MAPPO algorithm. The results are presented in Figure (1). We observe the following;

On the one hand, learning with a global reward signal can ensure the cooperation of agents. Among the two scenarios, the global reward settings both converge. However, the variance of the estimated gradient in environments with a high number of agents can be significantly high; this additional variance is the cost of the credit assignment from scalarization. In fact, any global-reward algorithms face a theoretical sample-efficiency limit that scales with the number of agents (Bagnell & Ng, 2005), exacerbating the credit assignment problems (Foerster et al., 2018; Kuba et al., 2021). Existing works alleviate this problem either through adaptive trust region (Sun et al., 2022), sequential updates (Zhong et al., 2024), or conservative update mechanisms (Wu et al., 2021).

On the other hand, learning with separate reward signals can converge faster, especially in environments with a large number of agents, since local reward learning does not suffer from the credit assignment problem. However, the cost of this learning approach is the potential of suboptimal convergence (Devlin et al., 2014; Le & Ta, 2025). Resolving this problem generally requires careful reward engineering and experimentations (Mao et al., 2020).

We summarize our observation as the following *reward dilemma* for multi-agent RL

The credit assignment problem introduced by global reward scalarization imposes additional variance that scales with the number of agents, potentially slowing down the learning process. However, local reward learning can cause severe consequences due to miscoordination.

From this observation, we see the limitations of both the global scalarization and local reward learning. Restricting learning to only one of these settings can be insufficient for a truly general learning framework. This motivates the development of a framework that supports more flexible learning paradigms, allowing a smooth transition between these two extremes. In this work, we take a step in this direction. Our approach can offer greater flexibility to reward settings and facilitate more effective optimization in MARL, while mitigating the credit assignment issues of global rewards and the miscoordination risks associated with purely local rewards.

5. Method

5.1. Dependence Graph Policy Gradient

We now derive how the dependence structure introduced in the previous section enables a more efficient computation of the policy gradient. Our starting point is the fully cooperative objective, where all agents jointly aim to maximize the total expected cumulative reward,

$$\mathcal{J}(\pi) = \sum_{i=1}^N \mathcal{J}^i(\pi), \quad \mathcal{J}^i(\pi) := \mathbb{E}_\pi \sum_{t=0}^{\infty} \gamma^t r_t^i.$$

The policy gradient with respect to agent j 's parameters can then be written as $\nabla_{\pi_j} \mathcal{J}(\pi) = \sum_{i=1}^N \nabla_{\pi_j} \mathcal{J}^i(\pi)$. Each term $\nabla_{\pi_j} \mathcal{J}^i(\pi)$ is the cross-agent gradient that captures the rate of change at which agent j 's policy influences the agent i 's objective. Using the multi-agent policy gradient theorem (Foerster et al., 2018; Kuba et al., 2021), we have

$$\nabla_{\pi_j} \mathcal{J}^i(\pi) = \mathbb{E}_{\rho_\pi, \pi} \left[\nabla \log \pi_j(a^j | s^j) Q_\pi^i(s, a) \right], \quad (1)$$

where $Q_\pi^i(s, a)$ denotes the joint action-value function of agent i under the joint policy π . In local reward settings, the

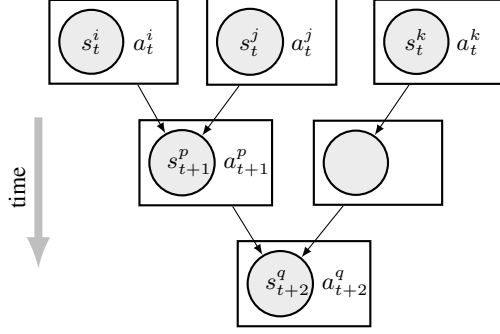


Figure 2. An example of an MDP with decomposed state structure. Agent k (top right) cannot influence agent q at timestep $t + 1$; any effect can only occur from timestep $t + 2$ onward (bottom). Since agent q lies in agent k 's blind spot, it can be excluded from the gradient computation at $t + 1$.

cross-agent gradients are completely ignored; i.e. $\nabla_{\pi_i} \mathcal{J}^j = 0, \forall j \neq i$.

With the dependence graph, we can further simplify the policy gradient in (1) to include only the necessary states that affect agent i 's rewards. As illustrated in Figure 2, if agent k takes an action at timestep t , it cannot directly affect the state of agent p at timestep $t + 1$ as there is no edge connecting them. Therefore, the gradient of agent p 's reward with respect to agent k 's action is zero in this case. However, the state of agent q at time $t + 2$ can be influenced by agent k , but only through an intermediate state, which is an indirect effect that "propagates" from agent k through paths on the graph. We formalize this as follows.

Proposition 5.1. Fix a joint policy π . Let $i, j \in \mathcal{N}$. The policy gradient $\nabla_{\pi_j} \mathcal{J}^i(\pi)$ is given by

$$\mathbb{E}_{\rho_{\pi}, \pi} \left[\nabla \log \pi_j(a_0^j | s_0^j) \mathbb{E}_{\tau} \left[\sum_{k \geq t'} \gamma^k r^i(s_k^i, a_k^i) \middle| \mathbf{s}_0, \mathbf{a}_0 \right] \right], \quad (2)$$

where t' is the first timestep where there is a path from (\mathbf{s}_0, j) to $(\mathbf{s}_{t'}, i)$ in a trajectory τ . A path is defined as in definition 3.3.

We call the policy gradient that is estimated through Proposition 5.1 the *dependency-graph* policy gradient, and denote it by $\nabla_{\pi_j} \mathcal{J}(\pi; \mathcal{G})$. Compared to the traditional policy gradient, equation (2) differs by the cumulative reward that only starts after the timestep t' . As a result, if each agent operates relatively independently, i.e., a sparse dependence graph, then the cross-agent gradient can become exponentially small based on the meeting timestep. On the contrary, if all agents' MDPs are tightly coupled, e.g., a fully connected dependence graph, then (2) returns to a vanilla policy gradient. In practical implementations, equation (2) provides a principled way to restrict gradient estimation to the set of agents and timesteps that causally influence

Algorithm 1 Policy Gradient with Multi-Agent GAE- λ and Dependence Graph

input Trajectory $\tau = \{(\mathbf{s}_t, r_t^i)\}_{t=0}^{T-1}$, value estimates $\{V^i(\mathbf{s}_t)\}_{t=0}^T$, discount factor γ , GAE parameter λ , adjacency matrix $\{\mathbf{A}^t\}_{t=0}^{T-1}$, action scores $\{\nabla \log(\pi_j(a_t^j | s_t^j))\}_{t=0}^{T-1}$
output Gradient $\hat{\nabla}_{\pi_j} \mathcal{J}^i(\pi; \mathcal{G})$, Advantage $\{A_t^i\}_{t=0}^{T-1}$

- 1: Initialize $A_t \leftarrow 0$ for all $t = 0, \dots, T - 1$
- 2: **for** $t_0 = T - 1$ **down to** 0 **do**
- 3: $gae \leftarrow 0$
- 4: $H \leftarrow \text{diag}(1)$
- 5: **for** $t = t_0$ **to** $T - 1$ **do**
- 6: $\delta_t^i \leftarrow r_t^i + \gamma V^i(\mathbf{s}_{t+1}) - V^i(\mathbf{s}_t)$
- 7: $H \leftarrow H \cdot \mathbf{A}^t$
- 8: $gae \leftarrow \delta_t^i (\gamma \lambda)^{t-t_0} (\lambda \mathbf{1}(H_{ji} > 0) + 1 - \lambda) + gae$
- 9: **end for**
- 10: $A_{t_0}^i \leftarrow gae$
- 11: **end for**

return $\frac{1}{T} \sum_{t=0}^{T-1} \gamma^t A_t^i \nabla \log \pi_j(a_t^j | s_t^j), \{A_t^i\}_{t=0}^{T-1}$

one another, i.e, the credit assignment problem, potentially reducing the variance of the policy gradient.

Our dependency-graph Policy Gradient operates on an orthogonal dimension and is complementary to the Policy gradient with Networked MDPs in the prior works. More specifically, compared to Lemma 2 in Qu et al. (2020), where the joint value functions are approximated through a small subset of k -hop parents, with the approximation error reducing exponentially fast with k , i.e., the value function *representation* dimension. Our policy gradient operates on the *time* dimension where the value functions can be estimated after the meeting timestep t' , without changing the gradient. Practically, we still use the global value representation in our implementation, which we illustrate in Algorithm 1. Combining these two dimensions can be a promising direction and is left to future work. Our result on dependence paths also resembles the reachability concept in Multi-Agent Influence graphs (Koller & Milch, 2003).

5.2. Dependence Graph Estimation as a World Model learning problem

The formulation of the dependence graph \mathcal{G} introduced earlier assumes knowledge of the underlying transition dynamics \mathbf{P} . In practice, however, the transition model is often unknown or only partially observable, making it infeasible to construct the exact dependence graph. In fact, prior works either assume that the graph is given (Qu et al., 2020), or use predefined structures (Ma et al., 2024). In this section, we consider how an approximate graph \mathcal{G}' can be used in place of the true graph. We first establish a condition under which the resulting policy gradient remains accurate.

Lemma 5.2 (Gradient Error under an Approximated Dependence Graph). *Let \mathcal{G} be the true dependence graph induced by the transition kernel \mathbf{P} , and let \mathcal{G}' be an approximate graph for which there exists a transition kernel $\mathbf{P}'_{\mathcal{G}'}$, that admits \mathcal{G}' as its dependence graph and satisfies*

$$\sup_{\mathbf{s}, \mathbf{a}} \|\mathbf{P}(\cdot | \mathbf{s}, \mathbf{a}) - \mathbf{P}'_{\mathcal{G}'}(\cdot | \mathbf{s}, \mathbf{a})\|_1 \leq \varepsilon. \quad (3)$$

Let $\nabla_{\pi_j} \mathcal{J}(\pi; \mathcal{G}')$ denote the dependency-graph policy gradient from the graph \mathcal{G}' . If rewards are bounded in $[0, R_{\max}]$ and $B_j := \sup_{s^j, a^j} \|\nabla \log \pi_j(a^j | s^j)\|$ is finite, then

$$\|\nabla_{\pi_j} \mathcal{J}^i(\pi) - \nabla_{\pi_j} \mathcal{J}^i(\pi; \mathcal{G}')\| \leq O\left(B_j \frac{\gamma \varepsilon R_{\max}}{(1 - \gamma)^2}\right),$$

where the notation $O(\cdot)$ hides constant factors.

The subtlety of lemma 5.2 is the use of the approximated graph \mathcal{G}' instead of \mathcal{G} in the policy gradient while using samples from \mathbf{P} . The existence of the kernel $\mathbf{P}'_{\mathcal{G}'}$ is to only guarantee that \mathcal{G}' represents something sensible but is not used otherwise. Lemma 5.2 suggests a theoretical approach for estimating such a dependence graph through a model-based approach; by learning a dynamic model \mathbf{P}' , then the induced graph \mathcal{G}' gives small-bias estimation of the gradient as long as the model prediction error is small. However, directly estimating the total variation in (3) of the world model can be very challenging because it usually involves learning a high-dimensional, complex next-state distribution. Furthermore, it is unclear how to extract a dependence graph from a learned world model in practice. We next consider this quantity in a slightly different form.

For a given proper graph \mathcal{G}' , we let $\mathbf{P}_{\mathcal{G}'}$ be the probability of next states conditional on the graph structure of \mathcal{G}' , i.e.

$$P_{\mathcal{G}'}^i(s^{i'} | \mathbf{s}, \mathbf{a}) = P^i(s^{i'} | \{s^k, a^k : k \in \text{Pa}_{\mathcal{G}'}^i(\bar{s}^i)\}); \forall i \in [N].$$

When \mathcal{G}' encompasses all edges in \mathcal{G} , then $\mathbf{P}_{\mathcal{G}'}$ recovers \mathbf{P} , otherwise, $\mathbf{P}_{\mathcal{G}'}$ is a marginal probability of \mathbf{P} whose marginalization is edges present in \mathcal{G} but not in \mathcal{G}' . By definition, $\mathbf{P}_{\mathcal{G}'}$ is a transition kernel that admits \mathcal{G}' as its dependence graph (it is, in fact, the best approximated \mathbf{P}' on \mathcal{G}'). Pinsker's inequality gives us an upper bound

$$\mathbb{E} \|P^i - P_{\mathcal{G}'}^i\|_1 \leq \sqrt{2} \sum_{j, n=1}^N \mathbb{E} \left[\sqrt{I(S^{i'}; (S^j, A^j))} \middle| \text{Pa}_n^i(s^i) \right] \quad (4)$$

where $\{\text{Pa}_n^i\}_{n=1}^N$ is a collection of non-decreasing agent-dependence sets for each s^i such that $\text{Pa}_1^i(s^i) = \text{Pa}_{\mathbf{P}}^i(s^i) \cap \text{Pa}_{\mathcal{G}'}^i(s^i)$, $\text{Pa}_N^i(s^i) = \text{Pa}_{\mathbf{P}}^i(s^i)$, and $|\text{Pa}_{m+1}^i(s^i) \setminus \text{Pa}_m^i(s^i)| \leq 1$. Furthermore, with some abuse of notations, we denote $\text{Pa}^i(\cdot)$ the states and actions of agents in $\text{Pa}^i(\cdot)$. Full derivation and other details of this result are left to Appendix A.5. Intuitively, if agent i 's states and actions have

little impact on agent j 's future states, then the mutual information is low, and thus agent j can be considered not to be connected to agent i in the dependence graph. Additionally, if the agent j in \mathcal{G} is also included in the graph \mathcal{G}' , then the mutual information equals 0 since it is conditioned on all the correct dependence agents and thus does not contribute to the upper bound of model errors. As a special case, if $\text{Pa}_{\mathcal{G}'}^i(\cdot) \supseteq \text{Pa}_{\mathbf{P}}^i(\cdot)$, then the RHS of (4) is 0. As a result, we can construct \mathcal{G}' so that the upper bound in (4) is small, leading to small error gradients as in Lemma 5.2 while not having to learn \mathbf{P}' .

5.3. Approximating Dependence Graph via reverse world models

The procedure of the edge estimation in (4) is more practical than the total variation in (3). However, estimating the mutual information of general distributions remains statistically challenging (McAllester & Stratos, 2020). While methods exist for estimating the mutual information of general, high-dimensional distributions, they either have high variance (Belghazi et al., 2018) or are primarily used for representation learning (Oord et al., 2018). For this reason, we introduce two simplifications to the formulation to ease the mutual information estimation problem.

First, the mutual information in (4) can be written as $I(S^{i'}; S^j, A^j) = I(S^{i'}; S^j) + I(S^{i'}; A^j | S^j)$. As the MI between states $S^{i'}$ and S^j can be difficult to estimate, we will ignore the former term and assume that the next states only depend on the actions of other agents. Second, we approximate the states and actions in $\text{Pa}_n^i(s^i)$ with (s^i, a^i) . This approximation is accurate when the dependence graph has a low degree of vertices, such as 1 or 2. Overall, with these simplifications, our objective derived from (4) becomes

$$\begin{aligned} L_i(\pi) &:= \mathbb{E} \sum_j^N I(S^{i'}; A^j | S^i, A^i, S^j) \\ &= \mathbb{E} \sum_j^N [H(A^j | S^j) - H(A^j | S^i, S^j, S^{i'})]. \end{aligned} \quad (5)$$

To estimate the entropies in (5), we adopt a variational lower bound based on a learned reverse dynamics model. Specifically, we train (i) an action prediction model q_ϕ to estimate $\hat{H}_{q_\phi}(A^j | S^j)$ and (ii) a multi-agent reverse world model q_ψ that predicts agent j 's action conditioned on the state information of both agents i and j . To determine whether a directed edge from agent i to agent j exists at state \mathbf{s} , we compute the discrepancy between the two entropy terms. If conditioning on agent i significantly reduces the uncertainty of A^j , then we consider there is an edge between them. To construct \mathcal{G}' , we apply a soft thresholding as a

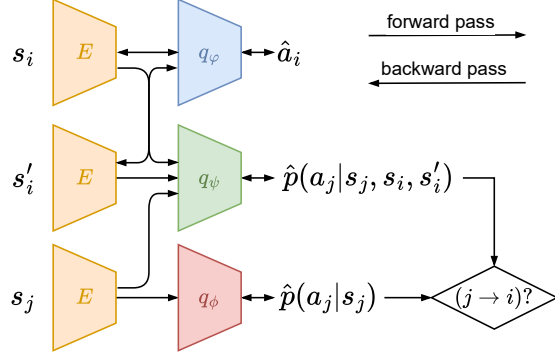


Figure 3. Dependence graph approximation via reverse world models.

heuristic rule to define an edge from j to i whenever

$$\frac{\hat{H}_{q_\psi}(A^j|s^i, s^j, s^{i'})}{\hat{H}_{q_\phi}(A^j|s^j)} < c,$$

where c is a hyperparameter in the range of $[0, 1]$. Also, by our assumption, we always include self-edges in the graph. The value of c can be used to control the density of the approximated graph \mathcal{G}' . At the extreme value $c = 0$, our method reverts to the standard local reward setup. In our experiments, we manually select c at 0.9 for all experiments.

5.4. Practical Implementation

Finally, to make our method more effective in practice, two additional challenges must be addressed. First, the approximated graph on the original state space may contain many spurious edges. For example, agents may partially observe other agents' local states, even when it does not have a direct impact on their future states; such observations can allow for more accurate prediction of other agents' actions, resulting in many redundant edges. Second, the approximated entropy difference in (5) is neither a lower nor an upper bound of the mutual information, as discussed in McAllester & Stratos (2020), which can lead to noisy graph approximations.

To mitigate the first issue, we adopt a learned latent state that filters out irrelevant information. Specifically, we train an encoder E that maps the original states to a latent space that captures the information relevant only to the current agent by using a single-agent reverse world model q_ϕ . This single-agent reverse world model guides the encoder to retain only the information that is necessary for the current agent while ignoring the extraneous information about others. Our overall model approximation scheme with reverse world models is illustrated in Figure 3.

To address the second issue, we devise an estimate strategy that combines multiple meeting timesteps t' . In particular, Proposition 5.1 shows that the true meeting timestep t' provides the tightest estimate; however, any other estimate

using a timestep earlier than t' will also have the same expected gradient. As a result, we compute an exponentially weighted average of the dependence-graph gradients over all meeting timesteps earlier than the approximated timestep t' . This aggregation scheme is analogous to GAE scheme, which results in a novel GAE-like estimate that incorporates the dependence graphs. The overall procedure is presented in Algorithm 1, with detailed derivations in Appendix A.4.

6. Experiments

We design our experiments to answer the following questions: 1) Does using the dependence graph improve the training efficiency? and 2) How good is the approximated dependence graph compared to other graph structures? We evaluate our methods on two popular MARL benchmarks, namely LBF and SMAClite, which we modified to support local reward settings. In LBF, we also add a more challenging setup where agents are required to cooperate to collect food, but the rewards are distributed to only the highest-level agent, with deterministic tie-breaks (winner takes all setup), making the credit attribution in the local reward setting more difficult. Due to space constraints, we defer the environment specification details to Appendix A.7. Since our method is compatible with any on-policy gradient method, we adopt our backbone algorithms on both MAPPO (Yu et al., 2022) and IPPO (De Witt et al., 2020) with Dependence Graph (DG). We compare our approach against the same algorithms under two other reward settings, namely global and local rewards. Furthermore, we also compare our method to IQL (local reward), QMIX (global reward) (Rashid et al., 2020b), and QPLEX (global reward) (Wang et al., 2020b) as other strong value-based baselines from both global and local reward settings. For a fair comparison, all methods utilize parameter sharing between agents. Detailed network architecture and hyperparameter settings are provided in Appendix A.8. Our source code is publicly available ¹.

6.1. Results

Figure 4 presents the results on the LBF benchmark. Our method consistently improves performance for both IPPO and MAPPO, achieving the best results among all baselines. Specifically, using the Dependence Graph, IPPO increases its interquartile mean (IQM) reward to 0.89, compared to 0.66 with local rewards and 0.68 with global rewards. MAPPO shows a similar trend: IQM improves to 0.85 with the Dependence Graph, compared to 0.58 under local rewards and 0.77 under global rewards. Interestingly, under the same reward setups, IPPO performs better than MAPPO under local rewards, whereas MAPPO outperforms IPPO with global rewards. Dependence Graph yields slightly larger gains for IPPO than for MAPPO, possibly due to

¹<https://github.com/giangbang/dependence-graph-epymarl>

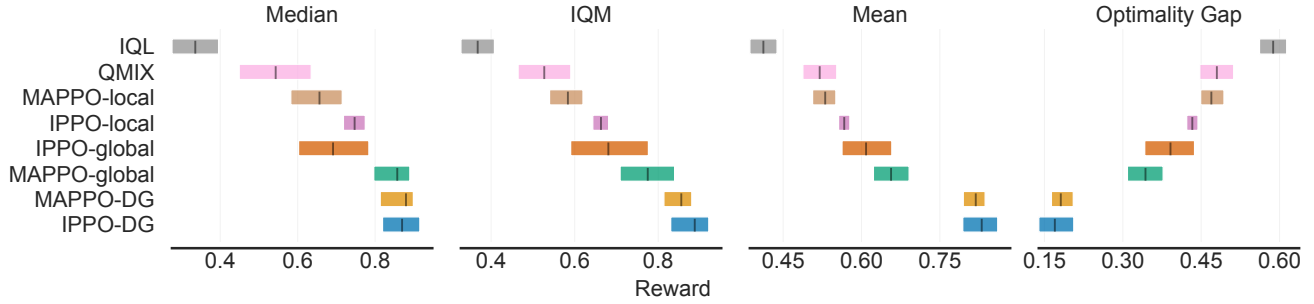


Figure 4. Results on the LBF benchmark on 6 selected scenarios. We follow the evaluation protocol recommended in Agarwal et al. (2021). Methods with dependence graphs consistently outperform other baselines from both local and global reward settings.

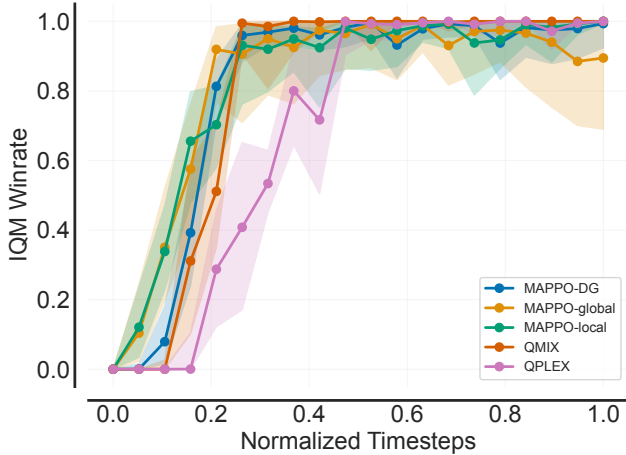


Figure 5. Result on the SMAClite benchmark on 6 scenarios. Overall, the performances of all methods are relatively comparable.

IPPO’s stronger performance under the local reward setup. Full experimental results are provided in Appendix A.9.

In SMAClite, while all methods generally achieve comparable performance, their results are very noisy throughout training. Therefore, we plot in Figure 5 the learning curve over the entire training process instead of reporting only the final result. QPLEX shows a slower initial learning phase but eventually converges to an optimal performance level. Overall, our findings are consistent with (Michalski et al., 2023), where MAPPO-based methods experience noisier training than value-based methods. Nevertheless, our approach improves training stability over both reward settings.

6.2. Ablation study on different graph structures

To examine the effect of the dependence graph on the efficiency of the proposed method, we conduct additional studies on MAPPO with different graph structures in the LBF benchmark. As baselines, we choose random graph structures where each agent has a probability of p that it connects to the other agents, also known as the Erdos-Renyi graph. We tested with different values of p corresponding

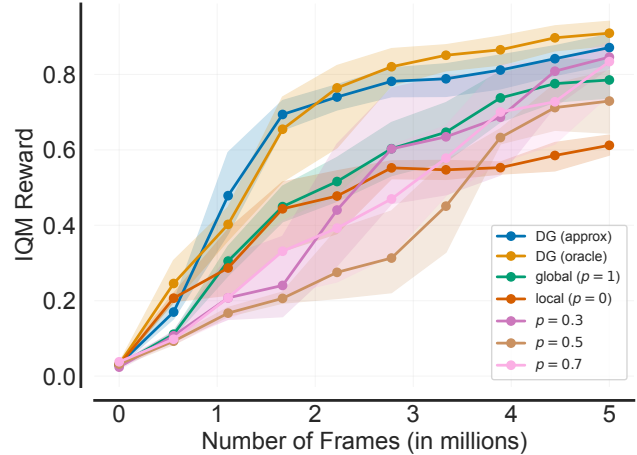


Figure 6. Ablation study on different graph structures. We test our methods (DG) with various random dependence graph structures, where each agent has a probability of p to form an edge with any other agent at any state. Global and local reward settings can be considered as special cases of random graphs with $p = 1$ and $p = 0$, respectively. Oracle graph is also provided as a baseline.

from sparse to dense graph connections. Furthermore, we also construct an oracle dependence graph setup based on domain knowledge of the LBF transitions. Specifically, we consider two agents connected if their L1 distances are less than or equal to 2. If there are multiple such agents, we only keep the two closest ones. Figure 6 demonstrates the effectiveness of our graph approximation, which performs almost comparably with the oracle graphs in this benchmark.

7. Conclusions

In this work, we present a MARL framework that leverages dependence graphs that capture dependencies between agents and their local states to filter irrelevant reward signals and mitigate credit assignment. We also propose a practical method that remains effective under noisy approximated graphs. Experiments show that our approach performs competitively across both local and global reward settings, offering a robust balance between the two approaches.

8. Impact Statement

This paper presents work whose goal is to advance the field of Machine Learning. There are many potential societal consequences of our work, none of which we feel must be specifically highlighted here.

References

Agarwal, A., Jiang, N., Kakade, S. M., and Sun, W. Reinforcement learning: Theory and algorithms. *CS Dept., UW Seattle, Seattle, WA, USA, Tech. Rep.*, 32:96, 2019.

Agarwal, R., Schwarzer, M., Castro, P. S., Courville, A. C., and Bellemare, M. Deep reinforcement learning at the edge of the statistical precipice. *Advances in neural information processing systems*, 34:29304–29320, 2021.

Ba, J. L., Kiros, J. R., and Hinton, G. E. Layer normalization. *arXiv preprint arXiv:1607.06450*, 2016.

Bagnell, D. and Ng, A. On local rewards and scaling distributed reinforcement learning. *Advances in Neural Information Processing Systems*, 18, 2005.

Belghazi, M. I., Baratin, A., Rajeshwar, S., Ozair, S., Bengio, Y., Courville, A., and Hjelm, D. Mutual information neural estimation. In *International conference on machine learning*, pp. 531–540. PMLR, 2018.

Böhmer, W., Kurin, V., and Whiteson, S. Deep coordination graphs. In *International Conference on Machine Learning*, pp. 980–991. PMLR, 2020.

Cao, Y., Yu, W., Ren, W., and Chen, G. An overview of recent progress in the study of distributed multi-agent coordination. *IEEE Transactions on Industrial informatics*, 9(1):427–438, 2012.

Chang, Y.-H., Ho, T., and Kaelbling, L. All learning is local: Multi-agent learning in global reward games. *Advances in neural information processing systems*, 16, 2003.

Christianos, F., Schäfer, L., and Albrecht, S. Shared experience actor-critic for multi-agent reinforcement learning. *Advances in neural information processing systems*, 33: 10707–10717, 2020.

De Witt, C. S., Gupta, T., Makoviichuk, D., Makoviychuk, V., Torr, P. H., Sun, M., and Whiteson, S. Is independent learning all you need in the starcraft multi-agent challenge? *arXiv preprint arXiv:2011.09533*, 2020.

Devlin, S., Yliniemi, L., Kudenko, D., and Tumer, K. Potential-based difference rewards for multiagent reinforcement learning. In *Proceedings of the 2014 international conference on Autonomous agents and multi-agent systems*, pp. 165–172, 2014.

Foerster, J., Farquhar, G., Afouras, T., Nardelli, N., and Whiteson, S. Counterfactual multi-agent policy gradients. In *Proceedings of the AAAI conference on artificial intelligence*, volume 32, 2018.

Gronauer, S. and Diepold, K. Multi-agent deep reinforcement learning: a survey. *Artificial Intelligence Review*, 55(2):895–943, 2022.

Guestrin, C., Koller, D., and Parr, R. Multiagent planning with factored mdps. *Advances in neural information processing systems*, 14, 2001.

Hernandez-Leal, P., Kaisers, M., Baarslag, T., and De Cote, E. M. A survey of learning in multiagent environments: Dealing with non-stationarity. *arXiv preprint arXiv:1707.09183*, 2017.

Hong, Y., Jin, Y., and Tang, Y. Rethinking individual global max in cooperative multi-agent reinforcement learning. *Advances in neural information processing systems*, 35: 32438–32449, 2022.

Hu, J., Jiang, S., Harding, S. A., Wu, H., and Liao, S.-w. Rethinking the implementation tricks and monotonicity constraint in cooperative multi-agent reinforcement learning. *arXiv preprint arXiv:2102.03479*, 2021.

Kok, J. R. and Vlassis, N. Collaborative multiagent reinforcement learning by payoff propagation. *Journal of machine learning research*, 7, 2006.

Koller, D. and Milch, B. Multi-agent influence diagrams for representing and solving games. *Games and economic behavior*, 45(1):181–221, 2003.

Kuba, J. G., Wen, M., Meng, L., Zhang, H., Mguni, D., Wang, J., Yang, Y., et al. Settling the variance of multi-agent policy gradients. *Advances in Neural Information Processing Systems*, 34:13458–13470, 2021.

Le, B. G. and Ta, V. C. Toward finding strong pareto optimal policies in multi-agent reinforcement learning. *Machine Learning*, 114(3):1–20, 2025.

Leibo, J. Z., Zambaldi, V., Lanctot, M., Marecki, J., and Graepel, T. Multi-agent reinforcement learning in sequential social dilemmas. *arXiv preprint arXiv:1702.03037*, 2017.

Lin, Y., Qu, G., Huang, L., and Wierman, A. Multi-agent reinforcement learning in stochastic networked systems. *Advances in neural information processing systems*, 34: 7825–7837, 2021.

Lowe, R., Wu, Y. I., Tamar, A., Harb, J., Pieter Abbeel, O., and Mordatch, I. Multi-agent actor-critic for mixed cooperative-competitive environments. *Advances in neural information processing systems*, 30, 2017.

Ma, C., Li, A., Du, Y., Dong, H., and Yang, Y. Efficient and scalable reinforcement learning for large-scale network control. *Nature Machine Intelligence*, 6(9):1006–1020, 2024.

Mao, H., Gong, Z., and Xiao, Z. Reward design in cooperative multi-agent reinforcement learning for packet routing. *arXiv preprint arXiv:2003.03433*, 2020.

McAllester, D. and Stratos, K. Formal limitations on the measurement of mutual information. In *International Conference on Artificial Intelligence and Statistics*, pp. 875–884. PMLR, 2020.

Michalski, A., Christianos, F., and Albrecht, S. V. Smaclite: A lightweight environment for multi-agent reinforcement learning. *arXiv preprint arXiv:2305.05566*, 2023.

Oord, A. v. d., Li, Y., and Vinyals, O. Representation learning with contrastive predictive coding. *arXiv preprint arXiv:1807.03748*, 2018.

Oroojlooy, A. and Hajinezhad, D. A review of cooperative multi-agent deep reinforcement learning. *Applied Intelligence*, 53(11):13677–13722, 2023.

Pan, A., Bhatia, K., and Steinhardt, J. The effects of reward misspecification: Mapping and mitigating misaligned models. *arXiv preprint arXiv:2201.03544*, 2022.

Papoudakis, G., Christianos, F., Schäfer, L., and Albrecht, S. V. Benchmarking multi-agent deep reinforcement learning algorithms in cooperative tasks. *arXiv preprint arXiv:2006.07869*, 2020.

Qu, G. and Li, N. Exploiting fast decaying and locality in multi-agent mdp with tree dependence structure. In *2019 IEEE 58th conference on decision and control (CDC)*, pp. 6479–6486. IEEE, 2019.

Qu, G., Lin, Y., Wierman, A., and Li, N. Scalable multi-agent reinforcement learning for networked systems with average reward. *Advances in Neural Information Processing Systems*, 33:2074–2086, 2020.

Rashid, T., Farquhar, G., Peng, B., and Whiteson, S. Weighted qmix: Expanding monotonic value function factorisation for deep multi-agent reinforcement learning. *Advances in neural information processing systems*, 33:10199–10210, 2020a.

Rashid, T., Samvelyan, M., De Witt, C. S., Farquhar, G., Foerster, J., and Whiteson, S. Monotonic value function factorisation for deep multi-agent reinforcement learning. *Journal of Machine Learning Research*, 21(178):1–51, 2020b.

Samvelyan, M., Rashid, T., De Witt, C. S., Farquhar, G., Nardelli, N., Rudner, T. G., Hung, C.-M., Torr, P. H., Foerster, J., and Whiteson, S. The starcraft multi-agent challenge. *arXiv preprint arXiv:1902.04043*, 2019.

Schulman, J., Moritz, P., Levine, S., Jordan, M., and Abbeel, P. High-dimensional continuous control using generalized advantage estimation. *arXiv preprint arXiv:1506.02438*, 2015.

Shalev-Shwartz, S., Shammah, S., and Shashua, A. Safe, multi-agent, reinforcement learning for autonomous driving. *arXiv preprint arXiv:1610.03295*, 2016.

Sun, M., Devlin, S., Beck, J., Hofmann, K., and Whiteson, S. Trust region bounds for decentralized ppo under non-stationarity. *arXiv preprint arXiv:2202.00082*, 2022.

Sunehag, P., Lever, G., Gruslys, A., Czarnecki, W. M., Zambaldi, V., Jaderberg, M., Lanctot, M., Sonnerat, N., Leibo, J. Z., Tuyls, K., et al. Value-decomposition networks for cooperative multi-agent learning. *arXiv preprint arXiv:1706.05296*, 2017.

Sutton, R. S. and Barto, A. G. *Reinforcement learning: An introduction*. MIT press, 2018.

Tampuu, A., Matiisen, T., Kodelja, D., Kuzovkin, I., Korjus, K., Aru, J., Aru, J., and Vicente, R. Multiagent cooperation and competition with deep reinforcement learning. *PloS one*, 12(4):e0172395, 2017.

Tan, M. Multi-agent reinforcement learning: Independent vs. cooperative agents. In *Proceedings of the tenth international conference on machine learning*, pp. 330–337, 1993.

Wang, J., Ren, Z., Han, B., Ye, J., and Zhang, C. Towards understanding linear value decomposition in cooperative multi-agent q-learning. 2020a.

Wang, J., Ren, Z., Liu, T., Yu, Y., and Zhang, C. Qplex: Duplex dueling multi-agent q-learning. *arXiv preprint arXiv:2008.01062*, 2020b.

Wang, J., Zhang, Y., Kim, T.-K., and Gu, Y. Shapley q-value: A local reward approach to solve global reward games. In *Proceedings of the AAAI conference on artificial intelligence*, volume 34, pp. 7285–7292, 2020c.

Wang, J., Xu, W., Gu, Y., Song, W., and Green, T. C. Multi-agent reinforcement learning for active voltage control on power distribution networks. *Advances in neural information processing systems*, 34:3271–3284, 2021.

Wang, L., Yang, Z., and Wang, Z. Breaking the curse of many agents: Provable mean embedding q-iteration for mean-field reinforcement learning. In *International conference on machine learning*, pp. 10092–10103. PMLR, 2020d.

Wang, L., Zhang, Y., Hu, Y., Wang, W., Zhang, C., Gao, Y., Hao, J., Lv, T., and Fan, C. Individual reward assisted multi-agent reinforcement learning. In *International conference on machine learning*, pp. 23417–23432. PMLR, 2022.

Weaver, L. and Tao, N. The optimal reward baseline for gradient-based reinforcement learning. *arXiv preprint arXiv:1301.2315*, 2013.

Wu, C., Rajeswaran, A., Duan, Y., Kumar, V., Bayen, A. M., Kakade, S., Mordatch, I., and Abbeel, P. Variance reduction for policy gradient with action-dependent factorized baselines. *arXiv preprint arXiv:1803.07246*, 2018.

Wu, Z., Yu, C., Ye, D., Zhang, J., Zhuo, H. H., et al. Coordinated proximal policy optimization. *Advances in Neural Information Processing Systems*, 34:26437–26448, 2021.

Yu, C., Velu, A., Vinitsky, E., Gao, J., Wang, Y., Bayen, A., and Wu, Y. The surprising effectiveness of ppo in cooperative multi-agent games. *Advances in Neural Information Processing Systems*, 35:24611–24624, 2022.

Yuan, L., Zhang, Z., Li, L., Guan, C., and Yu, Y. A survey of progress on cooperative multi-agent reinforcement learning in open environment. *arXiv preprint arXiv:2312.01058*, 2023.

Zheng, L., Yang, J., Cai, H., Zhou, M., Zhang, W., Wang, J., and Yu, Y. Magent: A many-agent reinforcement learning platform for artificial collective intelligence. In *Proceedings of the AAAI conference on artificial intelligence*, volume 32, 2018.

Zhong, Y., Kuba, J. G., Feng, X., Hu, S., Ji, J., and Yang, Y. Heterogeneous-agent reinforcement learning. *Journal of Machine Learning Research*, 25(1-67):1, 2024.

Zhou, M., Liu, Z., Sui, P., Li, Y., and Chung, Y. Y. Learning implicit credit assignment for cooperative multi-agent reinforcement learning. *Advances in neural information processing systems*, 33:11853–11864, 2020.

A. Appendix

A.1. Multi-agent Policy Gradient

The extension of the policy gradient theorem to multi-agent learning is introduced and proved in (Foerster et al., 2018), which we reproduce here for completeness. From the single-agent policy gradient theorem, we have

$$\begin{aligned}\nabla_{\pi_i} J(\pi) &= \mathbb{E}[\nabla_{\pi_i} \log \pi(\mathbf{a}|\mathbf{s}) Q(\mathbf{s}, \mathbf{a})] \\ &= \mathbb{E}\left[\nabla_{\pi_i} \log \prod \pi_i(a^i|s^i) Q(\mathbf{s}, \mathbf{a})\right] \\ &= \mathbb{E}\left[\sum_i^N \nabla \log \pi_i(a^i|s^i) Q(\mathbf{s}, \mathbf{a})\right]\end{aligned}$$

where the second equality is based on the independent policy assumption. With weight sharing, the global gradient equals the sum of the gradients of individual agents. In case that we want to write the gradient of one agent to another, as in Eq. (1), we can set $r = r^i$; the global reward as the reward of agent i , and using the multi-agent policy gradient theorem as above.

A.2. Discussion and limitations

Compare with the fully cooperative setting. While our approach requires the additional local-reward information, which may not be available for all environments. It is common that the reward from the scalar reward team can be attributed to a specific agent. For example, in the SMAC benchmark, the reward of an agent is the damage it deals to the enemy units, or in the LBF benchmark, the reward corresponds to agents participating in the food foraging. Even when the reward cannot be attributed explicitly, we can always distribute it evenly among the team, which essentially reduces our setting to a fully cooperative one. Additionally, scalarization the rewards is a one-way operator, where any vector-valued reward can be transformed into a scalar team reward, but the converse is not possible. Furthermore, even when the individual reward signals are available, existing methods do not provide principled approaches to leverage this reward vector to mitigate the credit assignment problems. In contrast, our work offers a theory-grounded framework for incorporating individual reward information directly into the optimization of the team objective.

Limitations. Our approach to graph approximation depends on the assumption that the neighboring agents can be inferred from the local observation, which technically is difficult to satisfy in practice (see Appendix A.3 for a discussion). Furthermore, the effect of ignoring the state mutual information in Section 5.3 is unknown, and we expect it to fail in environments where the transition probabilities depend heavily on agents' states instead of actions.

A.3. Factorization of states in practice

Our theoretical ground for the graph approximation procedure is based on the assumption that an agent can infer their neighbor agents from observed states, as introduced in Section 3. This assumption naturally allows for the graph approximation idea based on world model learning. In essence, the decomposition graph requires that current substates contain enough information to determine which agents it can interact with that can influence its next states. Strictly speaking, this requirement can be difficult to meet in practice. We demonstrate this argument in an illustrated example in this section. More specifically, we consider a simplified environment in Figure 7. In this example, the states of each agent are the field of vision where it can observe which other agents are adjacent in their vicinity (the oval circle). Next states of one agent not only depend on the nearby agents, but can also depend on the outside agents that can jump into its vision. A decomposition graph that is built on this observation state alone can not fully capture such "outsider" influences. However, we can consider that their overall effect can be negligible if the events of outside agents' interference happen rarely. Additionally, our theory on dependence graph policy gradient still holds, given that we know the correct graph structures to compute paths.

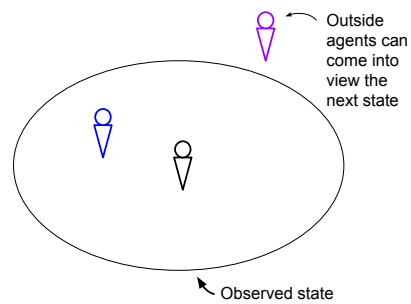


Figure 7. A simplified example, the purple agent can go into the observed states of the black agent and cannot be captured by a dependency graph based on the current substates of the black agent.

A.4. Multi-Agent GAE- λ with dependence graph

The key idea behind GAE is to average over all the n -step return estimations, which balances the high variance of Monte Carlo sampling and the high bias of the short-horizon n -step returns. We employ the same ideas as GAE for the meeting timestep t' , where we do not exclusively rely on a single estimate of this quantity. Similar to GAE, we start from the definition of TD error, defined as $\delta_t = r_t + \gamma V^i(s_{t+1}) - V^i(s_t)$, where $V^i(\cdot)$ are value estimates of the agent i 's policy. The multi-step advantage estimates from δ , combined with the dependence graphs at each timestep, are then defined as follows, for a given trajectory τ ,

$$\begin{aligned}\hat{A}_t^{(1)} &= \delta_t \\ \hat{A}_t^{(2)} &= 1(j \in \text{Pa}^i(s_t^i, 1, \tau))\delta_t + \gamma\delta_{t+1} \\ &\vdots \\ \hat{A}_t^{(k+1)} &= \sum_{l=0}^{k-1} \gamma^l 1(j \in \text{Pa}^i(s_{t+l}^i, l, \tau))\delta_{t+l} + \gamma^k \delta_{t+k},\end{aligned}$$

where $\text{Pa}^i(s_t, t, \tau)$ is the t -hop parents of s_t^i , defined in (7). Each of the $\hat{A}_t^{(k)}$ involves the sum of k TD error terms. Furthermore, all $\hat{A}_t^{(k)}$ are equivalent to advantage estimation with meeting times k upto $t' > k$, with t' the predicted first timestep that i and j are connected by a path. This can be effective for mitigating the noisy predictions of the dependence graphs inferred by the world models. Similar to GAE, we take the exponentially weighted average of all these terms

$$\begin{aligned}\hat{A}_t^{\text{GAE}} &= (1 - \lambda) \left(\hat{A}_t^{(1)} + \lambda \hat{A}_t^{(2)} + \lambda^2 \hat{A}_t^{(3)} + \dots \right) \\ &= (1 - \lambda) \left(\delta_t + \lambda \left(1(j \in \text{Pa}^i(s_t^i, t, \tau))\delta_t + \gamma\delta_{t+1} \right) \right. \\ &\quad \left. + \lambda^2 \left(1(j \in \text{Pa}^i(s_t^i, t, \tau))\delta_t + \gamma 1(j \in \text{Pa}^i(s_{t+1}^i, t+1, \tau))\delta_{t+1} + \gamma^2 \delta_{t+2} \right) + \dots \right) \\ &= (1 - \lambda) \left(\delta_t \left(1 + 1(j \in \text{Pa}^i(s_t^i, t, \tau))(\lambda + \lambda^2 + \dots) \right) \right. \\ &\quad \left. + \gamma \delta_{t+1} \left(\lambda + 1(j \in \text{Pa}^i(s_{t+1}^i, t+1, \tau))(\lambda^2 + \lambda^3 + \dots) \right) + \dots \right) \\ &= \lambda(1 - \lambda) \left(\delta_t \left(1(j \in \text{Pa}^i(s_t^i, t, \tau)) \right) (1 + \lambda + \lambda^2 + \dots) \right. \\ &\quad \left. + \gamma \delta_{t+1} \left(1(j \in \text{Pa}^i(s_{t+1}^i, t+1, \tau)) \right) (\lambda + \lambda^2 + \dots) + \dots \right) \\ &\quad + (1 - \lambda) \left(\delta_t + \gamma \lambda \delta_{t+1} + \dots \right) \\ &= \sum_{l=0}^{\infty} \gamma^l \lambda^{l+1} \delta_{t+l} \left(1(j \in \text{Pa}^i(s_{t+l}^i, t+l, \tau)) \right) + (1 - \lambda) \sum_{l=0}^{\infty} (\gamma \lambda)^l \delta_{t+l} \\ &= \sum_{l=0}^{\infty} (\gamma \lambda)^l \delta_{t+l} \left(\lambda \left(1(j \in \text{Pa}^i(s_{t+l}^i, t+l, \tau)) \right) + 1 - \lambda \right).\end{aligned}$$

Intuitively, when two agents are not connected by a path, we do not discard the contribution of the other agent's gradient entirely; instead, we downweight it by a factor of $1 - \lambda$. Finally, to find the t -hop parent set, we perform successive matrix multiplications of the adjacency matrices to the current timestep t as detailed in Algorithm 1.

A.5. Proofs

Proof of Proposition 5.1. From the policy gradient theorem, we unroll each timestep

$$\begin{aligned}
 \nabla_{\pi_j} \mathcal{J}^i(\boldsymbol{\pi}) &= \mathbb{E}_{\mathbf{s}_0 \sim \rho_{\boldsymbol{\pi}}, \mathbf{a}_0 \sim \boldsymbol{\pi}} [\nabla \log \pi_j(a_0^j | s_0^j) Q^i(\mathbf{s}_0, \mathbf{a}_0)] \\
 &= \mathbb{E}_{\rho, \boldsymbol{\pi}} \left[\nabla \log \pi_j(a_0^j | s_0^j) \left[\mathbb{E}[r_0^i(s_0^i, a_0^i)] + \gamma \mathbb{E}_{\mathbf{s}_1, \boldsymbol{\pi}} [Q^i(\mathbf{s}_1, \mathbf{a}_1) | \mathbf{s}_0, \mathbf{a}_0] \right] \right] \\
 &= \mathbb{E}_{\rho, \boldsymbol{\pi}} \left[\nabla \log \pi_j(a_0^j | s_0^j) \gamma \mathbb{E}_{\mathbf{s}_1, \boldsymbol{\pi}} [Q^i(\mathbf{s}_1, \mathbf{a}_1) | \mathbf{s}_0, \mathbf{a}_0] \right] \\
 &= \mathbb{E}_{\rho, \boldsymbol{\pi}} \left[\nabla \log \pi_j(a_0^j | s_0^j) \left[\gamma \mathbb{E}_{s_1^i, a_1^i} [r_1^i(s_1^i, a_1^i) | \mathbf{s}_0, \mathbf{a}_0] + \gamma^2 \mathbb{E}_{\mathbf{s}_2, \mathbf{a}_2} [Q^i(\mathbf{s}_2, \mathbf{a}_2) | \mathbf{s}_0, \mathbf{a}_0] \right] \right], \tag{6}
 \end{aligned}$$

where in the third equality, we use $\mathbb{E}_{a_0^i} [\nabla \log \pi_j(a_0^j | s_0^j) r_0^i(s_0^i, a_0^i)] = 0$ when $i \neq j$ (since we are assuming local reward structure), which we can write as

$$\nabla_{\pi_j} \mathcal{J}^i(\boldsymbol{\pi}) = \mathbb{E} \left[\nabla \log \pi_j(a_0^j | s_0^j) \mathbb{E}_{\tau} [r_0^i 1(j \in \{i\}) + \gamma Q^i(\mathbf{s}_1, \mathbf{a}_1) | \mathbf{s}_0, \mathbf{a}_0] \right].$$

Next, observe the first term in (6) that

$$\mathbb{E}_{s_1^i, a_1^i} [r_1^i(s_1^i, a_1^i) | \mathbf{s}_0, \mathbf{a}_0] = \sum_{s_1^i \in \mathcal{S}^i} \sum_{a_1^i \in \mathcal{A}^i} P^i(s_1^i | \{s_0^k, a_0^k : k \in \text{Pa}^i(s_0^i)\}) \pi_i(a_1^i | s_1^i) r_1^i(s_1^i, a_1^i)$$

So given \mathbf{s}_0 , if $j \notin \text{Pa}^i(s_0^i)$, then

$$\begin{aligned}
 &\mathbb{E}_{\mathbf{a}_0 \sim \boldsymbol{\pi}} \left[\nabla \log \pi_j(a_0^j | s_0^j) \mathbb{E}_{s_1^i, a_1^i} [r_1^i(s_1^i, a_1^i) | \mathbf{a}_0] \mid \mathbf{s}_0 \right] \\
 &= \mathbb{E}_{\mathbf{a}_0} \left[\nabla \log \pi_j(a_0^j | s_0^j) \mathbb{E}_{s_1^i, a_1^i} [r_1^i(s_1^i, a_1^i) | \mathbf{a}_0^{-j}] \mid \mathbf{s}_0 \right] \\
 &= 0.
 \end{aligned}$$

Note that we can interpret the property $j \notin \text{Pa}^i(s_0^i)$ as: given a segment of trajectory $\tau_{0:1} = (\mathbf{s}_0, \mathbf{s}_1)$ for an arbitrary $\mathbf{s}_1 \in \mathcal{S}$, then the path (defined on this segment of trajectory) $(\mathbf{s}_0, j) \rightarrow (\mathbf{s}_1, i)$ is not a path in the dependency graph. If this property holds, then the policy gradient of agent j with respect to the reward of agent i at the current timestep $t = 1$ is 0. In other word,

$$\nabla_{\pi_j} \mathcal{J}^i(\boldsymbol{\pi}) = \mathbb{E} \left[\nabla \log \pi_j(a_0^j | s_0^j) \mathbb{E}_{\tau} [r_0^i 1(j \in \{i\}) + \gamma r_1^i 1(j \in \text{Pa}^i(s_0^i)) + \gamma^2 Q^i(\mathbf{s}_2, \mathbf{a}_2) | \mathbf{s}_0, \mathbf{a}_0] \right].$$

We next consider the second term in (6)

$$\begin{aligned}
 &\mathbb{E}_{\rho, \boldsymbol{\pi}} \left[\nabla \log \pi_j(a_0^j | s_0^j) \left[\gamma^2 \mathbb{E}_{\mathbf{s}_2, \mathbf{a}_2} [Q^i(\mathbf{s}_2, \mathbf{a}_2) | \mathbf{s}_0, \mathbf{a}_0] \right] \right] \\
 &= \mathbb{E}_{\rho, \boldsymbol{\pi}} \left[\nabla \log \pi_j(a_0^j | s_0^j) \left[\gamma^2 \mathbb{E}_{s_2^i, a_2^i} [r_2^i(s_2^i, a_2^i) | \mathbf{s}_0, \mathbf{a}_0] + \gamma^3 \mathbb{E}_{\mathbf{s}_3, \mathbf{a}_3} [Q^i(\mathbf{s}_3, \mathbf{a}_3) | \mathbf{s}_0, \mathbf{a}_0] \right] \right].
 \end{aligned}$$

Again, we write the reward term in its explicit form

$$\begin{aligned}
 &\mathbb{E}_{s_2^i, a_2^i} [r_2^i(s_2^i, a_2^i) | \mathbf{s}_0, \mathbf{a}_0] \\
 &= \sum_{\mathbf{s}_1 \in \mathcal{S}} \sum_{\mathbf{a}_1 \in \mathcal{A}} \sum_{s_2^i \in \mathcal{S}^i} \sum_{a_2^i \in \mathcal{A}^i} \left[r_2^i(s_2^i, a_2^i) P^i(s_2^i | \{s_1^k, a_1^k : k \in \text{Pa}^i(s_1^i)\}) \pi_i(a_2^i | s_2^i) \right. \\
 &\quad \left. \prod_n^N \left[P^n(s_1^n | \{s_0^m, a_0^m : m \in \text{Pa}^n(s_0^n)\}) \pi_n(a_1^n | s_1^n) \right] \right] \\
 &= \sum_{\mathbf{s}_1 \in \mathcal{S}} \sum_{\mathbf{a}_1 \in \mathcal{A}} \sum_{s_2^i \in \mathcal{S}^i} \sum_{a_2^i \in \mathcal{A}^i} \left[r_2^i(s_2^i, a_2^i) P^i(s_2^i | \{s_1^k, a_1^k : k \in \text{Pa}^i(s_1^i)\}) \pi_i(a_2^i | s_2^i) \right. \\
 &\quad \left. \prod_{k \in \text{Pa}^i(s_1^i)} \left[P^k(s_1^k | \{s_0^m, a_0^m : m \in \text{Pa}^k(s_0^k)\}) \pi_k(a_1^k | s_1^k) \right] \right],
 \end{aligned}$$

the second equality is due to the marginal expectation of agents that are not in $\text{Pa}^i(s_1^i)$. So given \mathbf{s}_0 and \mathbf{s}_1 , if $j \notin \cup_{k \in \text{Pa}^i(s_1^i)} \text{Pa}^k(s_0^k)$, then

$$\mathbb{E}_{\mathbf{a}_0 \sim \boldsymbol{\pi}} \left[\nabla \log \pi_j(a_0^j | s_0^j) \mathbb{E}_{s_2^i, a_2^i} [r(s_2^i, a_2^i) | \mathbf{a}_0, \mathbf{s}_1] \mid \mathbf{s}_0 \right] = 0,$$

we can interpret the property $j \notin \cup_{k \in \text{Pa}^i(s_1^i)} \text{Pa}^k(s_0^k)$ as: given a segment of trajectory $\tau_{0:2} = (\mathbf{s}_0, \mathbf{s}_1, \mathbf{s}_2)$ for an arbitrary $\mathbf{s}_2 \in \mathcal{S}$, then all the paths (defined on this segment of trajectory) $(\mathbf{s}_0, j) \rightarrow (\mathbf{s}_1, \cdot) \rightarrow (\mathbf{s}_2, i)$ is not a path in the dependency graph \mathcal{G} . If this property holds, then the policy gradient of agent j with respect to the reward of agent i at the current timestep $t = 2$ is 0. In other word,

$$\begin{aligned} \nabla_{\pi_j} \mathcal{J}^i(\boldsymbol{\pi}) &= \mathbb{E} \left[\nabla \log \pi_j(a_0^j | s_0^j) \mathbb{E}_{\tau} \left[r_0^i \mathbf{1}(j \in \{i\}) + \gamma r_1^i \mathbf{1}(j \in \text{Pa}^i(s_0^i)) \right. \right. \\ &\quad \left. \left. + \gamma^2 r_2^i \mathbf{1}(j \in \cup_{m \in \text{Pa}^i(s_1^i)} \text{Pa}^m(s_0^m)) + \gamma^3 Q^i(\mathbf{s}_3, \mathbf{a}_3) | \mathbf{s}_0, \mathbf{a}_0 \right] \right]. \end{aligned}$$

Also, notice that $\cup_{k \in \text{Pa}^i(s_1^i)} \text{Pa}^k(s_0^k)$ is the set of 2-hop parents of s_0^i on the realised trajectory τ .

In general, with trajectories of states $\tau = (\mathbf{s}_0, \mathbf{s}_1, \mathbf{s}_2, \dots)$, by repeating the above steps, we can write the policy gradient as

$$\nabla_{\pi_j} \mathcal{J}^i(\boldsymbol{\pi}) = \mathbb{E}_{\mathbf{s}_0 \sim \rho_{\boldsymbol{\pi}}, \mathbf{a}_0 \sim \boldsymbol{\pi}} \left[\nabla \log \pi_j(a_0^j | s_0^j) \mathbb{E}_{\tau} \left[\sum_{t=0}^{\infty} \gamma^t r_t^i \mathbf{1}(j \in \text{Pa}^i(s_t^i, t, \tau)) \right] \right],$$

where we define $\text{Pa}^i(s_t^i, k, \tau)$ the k -hop parents of s_t^i on the trajectory τ , that is

$$\begin{aligned} \text{Pa}^i(s_t^i, k, \tau) &:= \text{Pa}^i(s_t^i, k-1, \tau) \cup \left(\bigcup_{m \in \text{Pa}^i(s_t^i, k-1, \tau)} \text{Pa}^m(s_{t-k}^m) \right) \\ &= \bigcup_{m \in \text{Pa}^i(s_t^i, k-1, \tau)} \text{Pa}^m(s_{t-k}^m), \end{aligned} \tag{7}$$

where the last equality is because $i \in \text{Pa}^i(s^i), \forall s^i \in \mathcal{S}^i$. As the base case, we define the 0-hop parents of any state as $\text{Pa}^i(s_t^i, 0, \tau) = \{i\}$.

Finally, we can see that the sets $\{\text{Pa}^i(s_t^i, t, \tau)\}_t$ is a non-decreasing sequence, because (7) can also be written as

$$\text{Pa}^i(s_t^i, t, \tau) = \bigcup_{n \in \text{Pa}^i(s_{t-1}^i)} \text{Pa}^n(s_{t-1}^n, t-1, \tau), \tag{8}$$

and that $i \in \text{Pa}^i(s_{t-1}^i)$. As a result, if there exists a timestep $t' > 0$ where $j \in \text{Pa}^i(s_{t'}^i, t', \tau)$, then all subsequent timesteps $t'' \geq t', j \in \text{Pa}^i(s_{t''}^i, t'', \tau)$. We can let t' be the smallest of such timesteps, in which case

$$\nabla_{\pi_j} \mathcal{J}^i(\boldsymbol{\pi}) = \mathbb{E}_{\rho_{\boldsymbol{\pi}}, \boldsymbol{\pi}} \left[\nabla \log \pi_j(a_0^j | s_0^j) \mathbb{E}_{\tau} \left[\sum_{k \geq t'} \gamma^k r^i(s_k^i, a_k^i) \mid \mathbf{s}_0, \mathbf{a}_0 \right] \right].$$

If there does not exist such timestep, then we can simply let $\nabla_{\pi_j} \mathcal{J}^i(\boldsymbol{\pi}) = 0$ on this trajectory, which is equivalent to $t' = \infty$. \square

Proof of Lemma 5.2. For fixed agents i and j , and a join policy $\boldsymbol{\pi}$, define the dependency-truncated value functions as

$$Q_{\mathbf{P}, \mathcal{G}}^{i,j}(\mathbf{s}, \mathbf{a}) := \mathbb{E}_{\tau \sim \mathbf{P}, \boldsymbol{\pi}} \left[\sum_{t=t'}^{\infty} \gamma^t r_t^i \mid \mathbf{s}_0 = \mathbf{s}, \mathbf{a}_0 = \mathbf{a} \right] \tag{9}$$

$$= \mathbb{E}_{\tau \sim \mathbf{P}, \boldsymbol{\pi}} \left[\sum_{t=0}^{\infty} \gamma^t r_t^i \mathbf{1}(j \in \text{Pa}^i(s_t^i, t, \tau)) \mid \mathbf{s}_0 = \mathbf{s}, \mathbf{a}_0 = \mathbf{a} \right], \tag{10}$$

where $t'(\tau, \mathcal{G}, \mathbf{s}_0, j, i)$ is the first timestep on trajectory τ at which there exists a directed path in graph \mathcal{G} from the originating vertex (\mathbf{s}_0, j) to $(\mathbf{s}_{t'}, i)$; if no such time exists we take the Q value to be zero, and $\text{Pa}^i(s_t^i, k, \tau)$ denotes the set of k -hop parents in the path to (\mathbf{s}_t, i) , i.e. $\text{Pa}^i(s_t^i, k, \tau) = \text{Pa}^i(s_t^i, k-1, \tau) \cup (\bigcup_{m \in \text{Pa}^i(s_t^i, k-1, \tau)} \text{Pa}^m(s_{t-k}^m))$ and $\text{Pa}^i(s_t^i, 0, \tau) = \{i\}$. Then,

$$\begin{aligned} & \nabla_{\pi_j} \mathcal{J}^i(\boldsymbol{\pi}; \mathcal{G}) - \nabla_{\pi_j} \mathcal{J}^i(\boldsymbol{\pi}; \mathcal{G}') \\ &= \mathbb{E}_{\rho_{\boldsymbol{\pi}}, \boldsymbol{\pi}} [\nabla \log \pi_j(a^j | s^j) (Q_{\mathbf{P}, \mathcal{G}}^{i,j}(\mathbf{s}, \mathbf{a}) - Q_{\mathbf{P}, \mathcal{G}'}^{i,j}(\mathbf{s}, \mathbf{a}))] \\ &= \mathbb{E}_{\rho_{\boldsymbol{\pi}}, \boldsymbol{\pi}} [\nabla \log \pi_j(a^j | s^j) (Q_{\mathbf{P}, \mathcal{G}}^{i,j}(\mathbf{s}, \mathbf{a}) - Q_{\mathbf{P}', \mathcal{G}'}^{i,j}(\mathbf{s}, \mathbf{a}) + Q_{\mathbf{P}', \mathcal{G}'}^{i,j}(\mathbf{s}, \mathbf{a}) - Q_{\mathbf{P}, \mathcal{G}'}^{i,j}(\mathbf{s}, \mathbf{a}))] \end{aligned}$$

Due to Proposition 5.1, we have $\nabla \log \pi_j(a^j | s^j) Q_{\mathbf{P}, \mathcal{G}}^{i,j}(\mathbf{s}, \mathbf{a}) = \nabla \log \pi_j(a^j | s^j) Q_{\mathbf{P}}^i(\mathbf{s}, \mathbf{a})$; where we denote $Q_{\mathbf{P}}$ the conventional Q value estimated on the transition kernel \mathbf{P} . As a result, using $\|\nabla \log \pi_j\| \leq B_j$ and a triangular inequality gives a standard bound

$$\begin{aligned} & \|\nabla_{\pi_j} \mathcal{J}(\boldsymbol{\pi}; \mathcal{G}) - \nabla_{\pi_j} \mathcal{J}(\boldsymbol{\pi}; \mathcal{G}')\| \\ & \leq B_j \underbrace{\left[\sup_{\mathbf{s}, \mathbf{a}} |Q_{\mathbf{P}}^i(\mathbf{s}, \mathbf{a}) - Q_{\mathbf{P}'}^i(\mathbf{s}, \mathbf{a})| \right]}_{T_1} \underbrace{\left[\sup_{\mathbf{s}, \mathbf{a}} |Q_{\mathbf{P}, \mathcal{G}'}^{i,j}(\mathbf{s}, \mathbf{a}) - Q_{\mathbf{P}', \mathcal{G}'}^{i,j}(\mathbf{s}, \mathbf{a})| \right]}_{T_2} \end{aligned}$$

Bound on T_1 . The bound in T_1 is a standard result in model-based learning. In particular, from the simulation lemma (see e.g. Lemma 2.2 in [Agarwal et al. \(2019\)](#)), one obtains

$$\sup_{\mathbf{s}, \mathbf{a}} |Q_{\mathbf{P}}^i(\mathbf{s}, \mathbf{a}) - Q_{\mathbf{P}'}^i(\mathbf{s}, \mathbf{a})| \leq \frac{\gamma \varepsilon R_{\max}}{(1-\gamma)^2}.$$

Bound on T_2 . To bound T_2 , we observe that given a trajectory τ and a proper graph \mathcal{G}' , then the estimated graph-truncated values do not depend on the underlying kernel; the difference only presents in the expectation with the difference in probability of trajectories. We start from the recursive form of $Q_{\mathbf{P}, \mathcal{G}}^{i,j}$ in (10), as

$$\begin{aligned} Q_{\mathbf{P}, \mathcal{G}}^{i,j}(\mathbf{s}, \mathbf{a}) &= \mathbb{E}_{\tau \sim \mathbf{P}, \boldsymbol{\pi}} \left[\sum_{t=0}^{\infty} \gamma^t r_t^i \mathbf{1}(j \in \text{Pa}^i(s_t^i, t, \tau)) \mid \mathbf{s}_0 = \mathbf{s}, \mathbf{a}_0 = \mathbf{a} \right] \\ &= \mathbb{E}_{\tau \sim \mathbf{P}, \boldsymbol{\pi}} \left[r_0^i \mathbf{1}(j \in \text{Pa}^i(s_0^i, 0, \tau)) + \sum_{t=1}^{\infty} \gamma^t r_t^i \mathbf{1}(j \in \text{Pa}^i(s_t^i, t, \tau)) \mid \mathbf{s}_0 = \mathbf{s}, \mathbf{a}_0 = \mathbf{a} \right] \\ &= \mathbb{E}_{\tau \sim \mathbf{P}, \boldsymbol{\pi}} \left[r_0^i \mathbf{1}(j \in \text{Pa}^i(s_0^i, 0, \tau)) + \gamma \sum_{t=1}^{\infty} \gamma^{t-1} r_t^i \left[\mathbf{1}(j \in \text{Pa}^i(s_t^i, t-1, \tau)) \right. \right. \\ &\quad \left. \left. + \mathbf{1} \left(j \in \bigcup_{k \in \text{Pa}^i(s_t^i, t-1, \tau)} \text{Pa}^k(s_0^k) \right) (1 - \mathbf{1}(j \in \text{Pa}^i(s_t^i, t-1, \tau))) \right] \mid \mathbf{s}_0 = \mathbf{s}, \mathbf{a}_0 = \mathbf{a} \right] \\ &= \mathbb{E} \left[r_0^i \mathbf{1}(j \in \text{Pa}^i(s_0^i, 0, \tau)) + \gamma Q_{\mathbf{P}, \mathcal{G}}^{i,j}(\mathbf{s}_1, \mathbf{a}_1) + \gamma^{t'} r_{t'} \mid \mathbf{s}_0 = \mathbf{s}, \mathbf{a}_0 = \mathbf{a} \right] \end{aligned}$$

where we use t' as shorthand for $t'(\tau, \mathcal{G}, \mathbf{s}_0, j, i)$. The last equality uses the definition of $Q^{i,j}$, and an observation that $\mathbf{1}(j \in \bigcup_{k \in \text{Pa}^i(s_t^i, t-1, \tau)} \text{Pa}^k(s_0^k)) (1 - \mathbf{1}(j \in \text{Pa}^i(s_t^i, t-1, \tau))) = 1$ only if j is not in the $(t-1)$ -hop parents to s_t^i , but is in

the t -hop parents, i.e. the definition of t' . Then,

$$\begin{aligned}
 & Q_{\mathbf{P}, \mathcal{G}'}^{i,j}(\mathbf{s}, \mathbf{a}) - Q_{\mathbf{P}', \mathcal{G}'}^{i,j}(\mathbf{s}, \mathbf{a}) \\
 &= \mathbb{E}[r^i | \mathbf{s}, \mathbf{a}] \mathbf{1}(j \in \text{Pa}^i(s^i, 0)) + \gamma \sum_{\mathbf{s}'} \mathbf{P}(\mathbf{s}' | \mathbf{s}, \mathbf{a}) \sum_{\mathbf{a}'} \boldsymbol{\pi}(\mathbf{a}' | \mathbf{s}') Q_{\mathbf{P}, \mathcal{G}'}^{i,j}(\mathbf{s}', \mathbf{a}') + \mathbb{E}_{\mathbf{P}, \boldsymbol{\pi}}[\gamma^{t'} r_{t'} | \mathbf{s}, \mathbf{a}] \\
 &\quad - \mathbb{E}[r^i | \mathbf{s}, \mathbf{a}] \mathbf{1}(j \in \text{Pa}^i(s^i, 0)) - \gamma \sum_{\mathbf{s}'} \mathbf{P}'(\mathbf{s}' | \mathbf{s}, \mathbf{a}) \sum_{\mathbf{a}'} \boldsymbol{\pi}(\mathbf{a}' | \mathbf{s}') Q_{\mathbf{P}', \mathcal{G}'}^{i,j}(\mathbf{s}', \mathbf{a}') - \mathbb{E}_{\mathbf{P}', \boldsymbol{\pi}}[\gamma^{t'} r_{t'} | \mathbf{s}, \mathbf{a}] \\
 &= \gamma \sum_{\mathbf{s}'} \left[\mathbf{P}(\mathbf{s}' | \mathbf{s}, \mathbf{a}) \sum_{\mathbf{a}'} \boldsymbol{\pi}(\mathbf{a}' | \mathbf{s}') Q_{\mathbf{P}, \mathcal{G}'}^{i,j}(\mathbf{s}', \mathbf{a}') - \mathbf{P}'(\mathbf{s}' | \mathbf{s}, \mathbf{a}) \sum_{\mathbf{a}'} \boldsymbol{\pi}(\mathbf{a}' | \mathbf{s}') Q_{\mathbf{P}', \mathcal{G}'}^{i,j}(\mathbf{s}', \mathbf{a}') \right] \\
 &\quad + \left[\mathbb{E}_{\mathbf{P}, \boldsymbol{\pi}}[\gamma^{t'} r_{t'} | \mathbf{s}, \mathbf{a}] - \mathbb{E}_{\mathbf{P}', \boldsymbol{\pi}}[\gamma^{t'} r_{t'} | \mathbf{s}, \mathbf{a}] \right].
 \end{aligned}$$

From the definition of $Q_{\mathbf{P}, \mathcal{G}}^{i,j}$; it is easy to see that $0 \leq Q_{\mathbf{P}, \mathcal{G}}^{i,j} \leq \frac{R_{\max}}{1-\gamma}$, then the first term of the above equation can be bounded by

$$\gamma \|\mathbf{P}(\cdot | \mathbf{s}, \mathbf{a}) - \mathbf{P}'(\cdot | \mathbf{s}, \mathbf{a})\|_1 \frac{R_{\max}}{1-\gamma} \leq \frac{\gamma \epsilon R_{\max}}{1-\gamma}.$$

For the second term, we observe that the timestep $t'(\tau, \mathcal{G}', \mathbf{s}, j, i)$ of a given trajectory τ is the same regardless of whether the underlying transition probability is \mathbf{P} or \mathbf{P}' , because we use the same graph \mathcal{G}' and the paths on this graph is unchanged. As a result, we can think of having both \mathbf{P} and \mathbf{P}' to have the same reward function, but this reward function is non-Markovian on the original state space because rewards are only bestowed on the first timestep when agents i and j are connected. For that reason, we cannot directly apply the simulation lemma argument as in T_1 . Fortunately, this can easily be fixed by augmenting the state space so that the rewards are Markovian on this new state space. More specifically, for an agent j , we augment each state \mathbf{s} with a vector of flags $\mathbf{f} \in \{0, 1\}^N$, indicating whether the agent j and other agents have already been connected. Let $\tilde{\mathbf{s}} = (\mathbf{s}, \mathbf{f})$. The augmented transition kernel can be defined as

$$\tilde{\mathbf{s}}_{t+1} = (\mathbf{s}_{t+1}, \mathbf{f}_{t+1}), \quad \mathbf{s}_{t+1} \sim \mathbf{P}(\cdot | \mathbf{s}_t, \mathbf{a}_t), \quad \mathbf{f}_{t+1}^i = \mathbf{1}\left(i \in \bigcup_{k: \mathbf{f}_t^k=1} \text{Pa}^k(s^k)\right), \quad \mathbf{f}_0^k = \begin{cases} 1 & k = j \\ 0 & k \neq j \end{cases}.$$

Under this augmented state space, the reward $r_{t'}$ is Markovian,

$$r_{t'}(\tilde{\mathbf{s}}_t, \mathbf{a}_t, \tilde{\mathbf{s}}_{t+1}) = r(\mathbf{s}_t, \mathbf{a}_t) \mathbf{1}(\mathbf{f}_t^i = 0 \wedge \mathbf{f}_{t+1}^i = 1),$$

Here, the indicator term denotes that the agent i is not connected to j in the current step but is in the next step. As a result, we can apply the same argument as in the bound T_1 by using the simulation lemma to conclude that

$$\sup_{\mathbf{s}, \mathbf{a}} \left| \mathbb{E}_{\mathbf{P}, \boldsymbol{\pi}}[\gamma^{t'} r_{t'} | \mathbf{s}, \mathbf{a}] - \mathbb{E}_{\mathbf{P}', \boldsymbol{\pi}}[\gamma^{t'} r_{t'} | \mathbf{s}, \mathbf{a}] \right| \leq \frac{\gamma \epsilon R_{\max}}{(1-\gamma)^2}.$$

Combining all the bounds, we get

$$\|\nabla_{\boldsymbol{\pi}_j} \mathcal{J}(\boldsymbol{\pi}; \mathcal{G}) - \nabla_{\boldsymbol{\pi}_j} \mathcal{J}(\boldsymbol{\pi}; \mathcal{G}')\| \leq \gamma \epsilon B_j R_{\max} \frac{3-\gamma}{(1-\gamma)^2} < \frac{3\gamma \epsilon B_j R_{\max}}{(1-\gamma)^2}.$$

□

Derivation of the inequality (4). Given the true graph \mathcal{G} and an approximated graph \mathcal{G}' . The transition kernel \mathbf{P} that is restricted to the graph structure of \mathcal{G}' can be defined as the marginal distribution:

$$P_{\mathcal{G}'}^i(s^i | \mathbf{s}, \mathbf{a}) = P^i(s^{i\prime} | s^i, a^k : k \in \text{Pa}_{\mathcal{G}'}^i(s^i)) \quad \forall i \in [N].$$

Now we consider two possible scenarios with the mismatch between \mathcal{G} and \mathcal{G}' :

1. \mathcal{G}' contains an edge that does not exist in \mathcal{G} . In other word, $\exists \mathbf{s} \in \mathcal{S}, i, j \in [N]$ such that $j \in \text{Pa}_{\mathcal{G}'}^i(\mathbf{s})$ and $j \notin \text{Pa}^i(\mathbf{s})$. In this case, since $\mathbf{P}_{\mathcal{G}}$ is the true transition kernel \mathbf{P} , conditioning \mathbf{P} on additional substate-action pairs does not change the next states distributions. As a result, this has no effect on the distribution of $\mathbf{P}_{\mathcal{G}}$.

2. \mathcal{G} contains an edge that does not exist in \mathcal{G}' . In this case, we are essentially predicting next states with missing information; $\mathbf{P}_{\mathcal{G}}$ is the average next states prediction marginalized on these missing edges.

As a result, we can safely ignore the former case and focus on the latter; we let for each state s^i , the set $\xi^i(s^i) = \text{Pa}^i(s^i) \setminus \text{Pa}_{\mathcal{G}'}^i(s^i)$. For simplicity, we assume that $|\xi^i(s^i)| = 1$; \mathcal{G} differs from \mathcal{G}' on only a single dependency agent at substate s^i . General cases can be easily expanded by a "bridging" argument; by gradually shrinking \mathcal{G} to \mathcal{G}' one edge at a time, which we will present later in the proof.

Let $m(s^i)$ be that missing agent, i.e. $\xi^i(s^i) = \{m(s^i)\}$. We then calculate the total variation of the difference between P^i and $P_{\mathcal{G}'}^i$ as

$$\begin{aligned} & \mathbb{E}_{\mathbf{s}, \mathbf{a}} \|P^i(\cdot | \mathbf{s}, \mathbf{a}) - P_{\mathcal{G}'}^i(\cdot | \mathbf{s}, \mathbf{a})\|_1 \\ &= \mathbb{E}_{\mathbf{s}, \mathbf{a}} \left\| P^i \left(\cdot | \{(s^k, a^k); k \in \text{Pa}_{\mathcal{G}'}^i(s^i)\} \cup \{(s^{m(s^i)}, a^{m(s^i)})\} \right) - P^i \left(\cdot | \{(s^k, a^k); k \in \text{Pa}_{\mathcal{G}'}^i(s^i)\} \right) \right\|_1 \\ &= \mathbb{E}_{s^i, a^i} \mathbb{E}_{(s, a)^{-i}, -m(s^i)} \mathbb{E}_{s^{m(s^i)}, a^{m(s^i)}} \left\| P^i \left(\cdot | \{(s^k, a^k); k \in \text{Pa}_{\mathcal{G}'}^i(s^i)\} \cup \{(s^{m(s^i)}, a^{m(s^i)})\} \right) - P^i \left(\cdot | \{(s^k, a^k); k \in \text{Pa}_{\mathcal{G}'}^i(\mathbf{s})\} \right) \right\|_1 \\ &\leq \sqrt{2} \mathbb{E} \mathbb{E}_{s^{m(s^i)}, a^{m(s^i)}} \left[D_{\text{KL}} \left[P^i \left(s^{i'} | \{(s^k, a^k); k \in \text{Pa}_{\mathcal{G}'}^i(s^i)\} \cup \{(s^{m(s^i)}, a^{m(s^i)})\} \right) \middle| P^i \left(s^{i'} | \{(s^k, a^k); k \in \text{Pa}_{\mathcal{G}'}^i(s^i)\} \right) \right]^{1/2} \right] \\ &\leq \sqrt{2} \mathbb{E}_{\mathbf{s}, \mathbf{a}} \left[I(S^{i'}; (S^{m(s^i)}, A^{m(s^i)}))^{1/2} \middle| \{(s^k, a^k); k \in \text{Pa}_{\mathcal{G}'}^i(\mathbf{s})\} \right] \\ &\leq \sqrt{2} \sum_j^N \mathbb{E}_{\mathbf{s}, \mathbf{a}} \left[I(S^{i'}; (S^j, A^j))^{1/2} \middle| \{(s^k, a^k); k \in \text{Pa}_{\mathcal{G}'}^i(\mathbf{s})\} \right], \end{aligned}$$

where the expectations are over the joint state and action distributions (of an arbitrary policy). The first inequality is due to Pinsker's inequality, the second inequality is a combination of Jensen's inequality (with square root) and the mutual information relation to the KL divergence. The last inequality is due to the fact that $m(s^i) \in [N]$.

Now, for a general graph \mathcal{G}' , we construct a sequence of graphs $\mathcal{G}_1, \mathcal{G}_2, \dots, \mathcal{G}_N$, where any two consecutive graphs differ from each other at most one edge at each state s^i , i.e. $|(\text{Pa}_{\mathcal{G}_n}^i \setminus \text{Pa}_{\mathcal{G}_{n+1}}^i)(s^i)| \leq 1$. By triangular inequality,

$$\begin{aligned} \mathbb{E} \|P^i - P_{\mathcal{G}'}^i\|_1 &\leq \mathbb{E} \|P^N - P_{\mathcal{G}'}^i\|_1 + \dots + \mathbb{E} \|P_{\mathcal{G}_1}^i - P^i\|_1 \\ &\leq \sqrt{2} \sum_n^N \mathbb{E} \left[\sum_j^N I(S^{i'}; (S^j, A^j))^{1/2} \middle| \{(S^k, A^k); k \in \text{Pa}_{\mathcal{G}_n}^i(\mathbf{s})\} \right]. \end{aligned}$$

□

A.6. Reward Dependence Graph

In addition to state transitions, agents may also interact through their immediate rewards. To capture such interactions, a reward-dependence graph can be defined that specifies how agents' actions influence one another's instantaneous rewards. Formally, we allow the reward of agent i to depend on the state-action pairs of a subset of agents, denoted by $\text{Pa}_{\text{rw}}^i \subseteq [N]$. Similar to the state-dependence set of the transition probabilities, the reward function of agent i can be defined in the same way as

$$r^i(\{s_k, a_k \mid k \in \text{Pa}_{\text{rw}}^i(s_i)\}) \in [0, R_{\max}].$$

Also, in this section only, we will denote $\text{Pa}_{\text{st}}^i(\cdot)$ as the state dependence sets to distinguish it from the reward dependence sets explicitly.

Proposition A.1. Fix a joint policy π . Let $i, j \in \mathcal{N}$. Let $\text{Pa}_{\text{rw}}^i(s_i)$ and $\text{Pa}_{\text{st}}^i(s_i)$ be the reward- and state-dependence agent set at state s_i of agent i , respectively. The policy gradient $\nabla_{\pi_j} \mathcal{J}^i(\pi)$ is given by

$$\mathbb{E}_{\rho_{\pi}, \pi} \left[\nabla \log \pi_j(a_0^j | s_0^j) \mathbb{E}_{\tau} \left[\sum_{t=0}^N \gamma^t r_t^i \mathbf{1}(j \in \text{Pa}^i(s_t^i, t, \tau)) \middle| \mathbf{s}_0, \mathbf{a}_0 \right] \right], \quad (11)$$

where $\text{Pa}^i(s_t^i, k, \tau)$ with $k > 0$ is the k -hop parents of s_t^i on the trajectory τ , defined as

$$\text{Pa}^i(s_t^i, k, \tau) = \bigcup_{m \in \text{Pa}^i(s_t^i, k-1, \tau)} \text{Pa}_{\text{st}}^m(s_{t-k}^m),$$

and we define the base-case of 0-hop parents as $\text{Pa}^i(s_t^i, 0, \tau) = \text{Pa}_{\text{rw}}^i(s_t^i)$. A path is defined according to the state dependence graph \mathcal{G} , similar to Proposition 5.1.

We note that the difference between this result and the result in 5.1 is the definition of k -hop parents. In particular, the 0-hop parents of an agent are initialized using the reward-dependence set, rather than the state-dependence graph alone. Proposition A.1 is strictly more general than proposition 5.1. Indeed, the 0-hop parent set defined in A.5 is a special case of $\text{Pa}^i(s_t^i, 0, \tau)$ under the local reward settings $\text{Pa}_{\text{rw}}^i(s_t^i) = \{i\}$. The proof of Proposition A.1 follows identically to that of Proposition 5.1 and is therefore omitted. Intuitively, the reward dependence set captures the immediate effects and thus contributes directly to the 0-hop parents. However, longer-term influences arise through the state-dependence graph, as state transitions propagate the effects of agents' states and actions into the future. Consequently, the parent sets are initialized by the reward-dependence sets and then expand recursively according to the state-dependence sets.

A.7. Environment and reward specifications

Level-Based Foraging (Christanos et al., 2020) is a suite of several gridworld-based environments, where the agents navigate to collect random spawned food across the map. Both agents and food have a level each, and the food is only collected if the sum of the levels of agents collecting it is larger than or equal to the level of the food. Rewards are assigned to agents upon collection based on their level of contribution to the collecting process.

Additionally, we consider a variation of the LBF benchmark. In this modified version, we introduce a more challenging reward structure that makes it harder for cooperative behavior among agents to emerge. Specifically, while the original LBF environment rewards each agent individually based on their level when collecting food, we adopt a winner-takes-all reward scheme: only the agent with the highest level receives a reward. In cases where multiple agents share the highest level, we break ties in a *deterministic* manner. Furthermore, the food levels are set so that at least two agents must cooperate to collect them (`-coop` setup). This setup penalizes myopic agents, while having no impact on approaches that rely on a global reward signal. We run our experiments on 3 scenarios from vanilla LBF and 3 scenarios with winner-take-all reward setups.

SMAClite (Michalski et al., 2023) is a fully open-source implementation of the popular SMAC benchmark (Samvelyan et al., 2019). SMAClite allows us to modify the environment to extract the agent-specific reward, which SMAC does not support. More specifically, the damage rewards are now attributed directly to the source agents that cause the damage. Other reward signals that cannot be attributed to a single source, for example, winning rewards and enemies' self-damage, are distributed evenly to all agents. Upon killing an enemy, the agents are rewarded with a large reward. As a result, while each agent is rewarded for the damage inflicted on the enemies, the local reward scheme can encourage the agents to "steal" kills from others. We run our experiments on 6 selected scenarios, ranging from large team coordination, such as 25m_vs_30m, to heterogeneous, role-specific scenarios like 3s5z_vs_3s6z.

A.8. Hyper-parameters Settings and Network Architecture

All the algorithms are based on the PyMARL framework (Papoudakis et al., 2020). As a result, all the hyperparameters used in this paper closely follow those reported in the framework. For a fair comparison, all PPO-based algorithms with different reward setups are GAE-enabled, with the GAE lambda λ set to 0.95 as recommended in (Schulman et al., 2015). Since SMAClite is not tested in the PyMARL, we follow suit SMAClite original paper (Michalski et al., 2023) to use the same hyperparameters of PyMARL for SMAC. For QMIX and QPLEX, we adopt the highly finetuned hyperparameters specifically for SMAC, as reported in (Hu et al., 2021), and used it in SMAClite. The full set of hyperparameters used in PPO-based methods is provided as follows.

All neural networks used in our experiments for the baseline methods, including the policy and value networks, follow the original PyMARL implementations without modification. In our method, the state encoder E is implemented as a three-layer neural network with hidden dimensions of 64 and an output dimension of 64. The single-agent reverse world model q_φ , the action predictor model q_ϕ , and the multi-agent reverse world model q_ϕ share the same architecture: a four-layer neural network with 256 neurons in the first hidden layer and 128 neurons in each of the remaining hidden layers. All networks use ReLU activations and Layer Normalization (Ba et al., 2016).

	SMAClite	LBF
hidden dimension	64	128
learning rate	0.0005	0.0005
reward standardisation	False	False
network type	GRU	FC
entropy coefficient	0.001	0.001
clip eps	0.2	0.2

Table 1. All PPO-based methods, including our MAPPO-DG and IPPO-DG, use the same hyperparameters that are adopted from PyMARL.

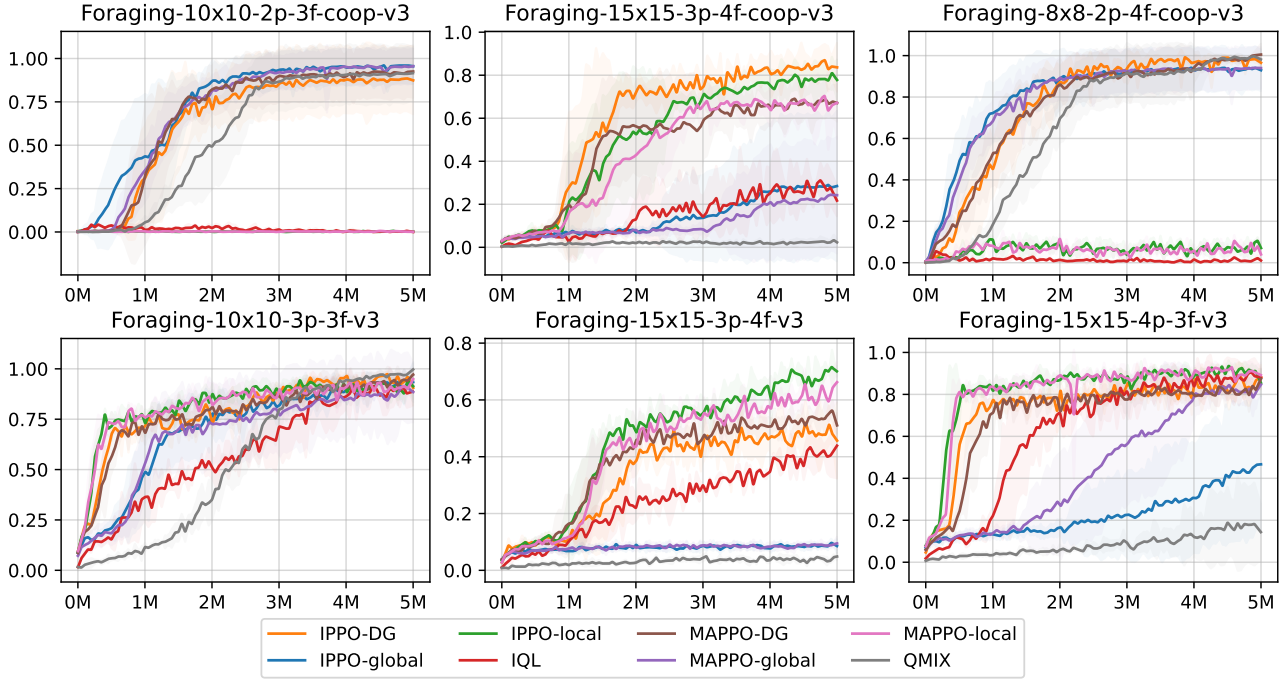


Figure 8. Full results on the LBF benchmark.

A.9. Detailed Experiment Results

Figure 8 presents the complete results corresponding to Figure 4 in the main paper. We can see that in the vanilla LBF scenarios (bottom row), agents trained with local reward signals consistently outperform those using global rewards. Especially in the 15x15-3p-4f environment, where all global methods, including MAPPO-global, QMIX, and IPPO-global struggle significantly due to the sparsity of the reward signals. In the 15x15-4p-3f setting, the addition of extra agents alleviates the sparsity issue to some extent, possibly due to the parameter sharing mechanism. MAPPO-global is able to converge to an optimal policy, albeit at a slower rate and with higher variance compared to the local reward setup. QMIX, on the other hand, fails to learn effectively even in this slightly less sparse scenario. IQL using local reward in this setting outperform QMIX with global rewards on all vanilla LBF setups except for in Foraging-10x10-3p-3f, where they both converge to optimal policies, but IQL learns a bit slower. In contrast, the winner-take-all with the cooperative setup (top row) poses challenges to the local reward approach. In this setup, due to the competitive nature of the reward function, the local reward approach struggles; it fails to learn in 2 out of 3 scenarios. Interestingly, some of the completely different branches of algorithms behave quite similarly under the same reward setting. In particular, in 10x10-2p-3f-coop and 8x8-2p-4f-coop, all local reward algorithms fail, including onpolicy methods with both MAPPO and IPPO, value-based method IQL, and value decomposition QMIX. In 15x15-3p-4f-coop, we observe a similar trend as in the winner-take-all setup, where an additional agent improves the performance of local reward with both value-based and onpolicy methods, except for QMIX. On the other hand, our method remains competitive across all the scenarios, demonstrating its robustness across different setups.

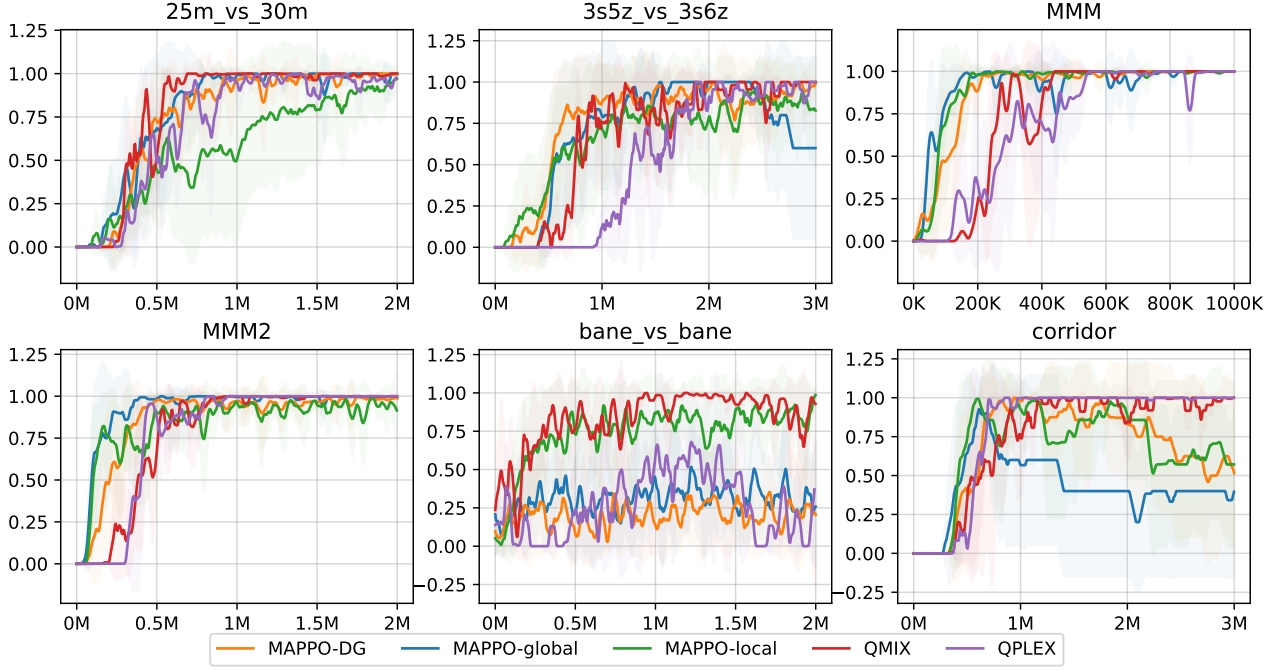


Figure 9. Full results on the SMAClite benchmark.

Figure (9) presents the full results on the SMAClite benchmark. QMIX achieves consistently strong performance across all scenarios. QPLEX performs quite similarly to QMIX, but slower in 3s5z_vs_3s6z and does not learn in bane_vs_bane. In most scenarios, our method and global MAPPO achieve comparable performance; for example, in 25m_vs_30m, both outperform local MAPPO. On corridor, however, our method and local MAPPO outperform global MAPPO. We attribute the unstable learning behavior observed in all MAPPO-based methods to suboptimal hyperparameters adopted from PyMARL.

A.10. Algorithm

Algorithm 2 Multi-Agent PPO (MAPPO and IPPO) with Dependence Graph.

```

1: Initialize shared actor parameters  $\theta$ , centralized critic parameters  $\vartheta$ , encoder  $E$ , single-agent reverse world model  $q_\varphi$ ,  

   action prediction model  $q_\phi$ , multi-agent reverse world model  $q_\psi$ 
2: for iteration = 1 to  $N_{\text{iter}}$  do
3:   Initialize empty buffer  $\mathcal{D}$ 
4:   for episode = 1 to  $N_{\text{episodes}}$  do
5:     for  $t$  = 1 to  $T$  do
6:       for each agent  $i = 1, \dots, N$  do
7:         Sample action  $a_t^i \sim \pi_\theta(\cdot | o_t^i)$ 
8:       end for
9:       Execute joint action  $\mathbf{a}_t = (a_t^1, \dots, a_t^N)$ 
10:      Observe rewards  $\{r_t^i\}$ , next state  $s_{t+1}$ , next obs  $\{o_{t+1}^i\}$ , done flag  $d_t$ 
11:      Store  $(s_t, o_t^i, a_t^i, r_t^i, \log p_t^i, d_t, s_{t+1})$  in  $\mathcal{D}$  for all  $i$ 
12:    end for
13:  end for
14:  for each timestep  $t$  in  $\mathcal{D}$  do
15:    Initialize Adjacency matrix  $\mathbf{A}_t = \text{diag}(1)$ 
16:    for each agent  $i$  in  $\mathcal{N}$  do
17:      Compute  $V_t^i = V_\vartheta^i(s_t)$  if MAPPO and  $V_\vartheta^i(o_t^i)$  if IPPO
18:      Compute latent state  $z_t^i = E(o_t^i)$ 
19:      Compute action distribution entropy  $H_1 = H(q_\phi(z_t^i))$ 
20:      for each agent  $j$  in  $\mathcal{N}$  do
21:        Compute latent state  $z_t^j = E(o_t^j)$ 
22:        Compute latent next state  $z_{t+1}^j = E(o_{t+1}^j)$ 
23:        Compute multi-agent reverse model distribution entropy  $H_2 = H(q_\psi(z_t^i, z_t^j, z_{t+1}^j))$ 
24:        Compute edge  $\mathbf{A}_{ij} = 1(H_2/H_1 < c)$ 
25:      end for
26:    end for
27:  end for
28:  Compute dependence truncated Advantage  $\{A_t^i\}_{t=0}^{T-1}$  in Algorithm 1 using  $\{V_t^i\}_{t=0}^{T-1}$  and  $\{\mathbf{A}_t^i\}_{t=0}^{T-1}$ 
29:  for epoch = 1 to  $K$  do
30:    for each minibatch  $\mathcal{B}$  do
31:      for each sample  $(o_t^i, a_t^i, \log p_t^i, A_t^i)$  in  $\mathcal{B}$  do
32:         $\log p^i = \log \pi_\theta(a_t^i | o_t^i)$ 
33:         $r^i = \exp(\log p^i - \log p_{\text{old}}^i)$ 
34:         $L_{\text{clip}}^i = \min(r^i A_t^i, \text{clip}(r^i, 1 - \epsilon, 1 + \epsilon) A_t^i)$ 
35:      end for
36:       $L_{\text{actor}} = -\frac{1}{|\mathcal{B}|} \sum_i L_{\text{clip}}^i$ 
37:       $L_{\text{critic}} = \frac{1}{|\mathcal{B}|} \sum (V_\vartheta^i(s) - V_{\text{target}}^i)^2$  if MAPPO and  $\frac{1}{|\mathcal{B}|} \sum (V_\vartheta^i(o^i) - V_{\text{target}}^i)^2$  if IPPO
38:       $L_{\text{entropy}} = -\beta \mathbb{E}[\mathcal{H}(\pi_\theta(\cdot | o^i))]$ 
39:       $L = L_{\text{actor}} + c_v L_{\text{critic}} + L_{\text{entropy}}$ 
40:      Update  $\theta, \vartheta$  using gradients of  $L$ 
41:    end for
42:  end for
43:  Compute latent states  $\{z_t^i\}_{t,i} = \{E(o_t^i)\}$ 
44:  Compute Encoder loss  $L_E = \frac{1}{|\mathcal{D}||\mathcal{N}|} \sum_{i,t} \text{CE}(q_\varphi(z_t^i, z_{t+1}^i), a_t^i)$ 
45:  Update Encoder  $E, \varphi$  using gradient of  $L_E$ 
46:  Detach gradient in  $\{z_t^i\}_{t,i}$ 
47:  Compute reverse model loss  $L_{\text{rv}} = \frac{1}{|\mathcal{D}||\mathcal{N}|^2} \sum_{i,j,t} [\text{CE}(q_\phi(z_t^i), a_t^i) + \text{CE}(q_\psi(z_t^i, z_t^j, z_{t+1}^j), a_t^i)]$ 
48:  Update  $\phi, \psi$  using gradient of  $L_{\text{rv}}$ 
49: end for

```
